RESERVOIR SIMULATION OF CO_2 SEQUESTRATION AND ENHANCED OIL RECOVERY IN THE TENSLEEP FORMATION, TEAPOT DOME FIELD

A Thesis

by

RICARDO GAVIRIA GARCIA

Submitted to the Office of Graduate Studies of
Texas A&M University
in partial fulfillment of the requirements for the degree of

MASTER OF SCIENCE

December 2005

Major Subject: Petroleum Engineering

RESERVOIR SIMULATION OF CO_2 SEQUESTRATION AND ENHANCED OIL RECOVERY IN THE TENSLEEP FORMATION, TEAPOT DOME FIELD

A Thesis

by

RICARDO GAVIRIA GARCIA

Submitted to the Office of Graduate Studies of
Texas A&M University
in partial fulfillment of the requirements for the degree of

MASTER OF SCIENCE

Approved by:

Chair of Committee, David Schechter
Committee Members, Daulat Mamora
Steven Dorobek
Head of Department, Stephen A. Holditch

December 2005

Major Subject: Petroleum Engineering

ABSTRACT

Reservoir Simulation of CO_2 Sequestration and Enhanced Oil Recovery in the Tensleep Formation, Teapot Dome Field. (December 2005)

Ricardo Gaviria Garcia, B.S., Universidad Industrial de Santander

Chair of Advisory Committee: Dr. David Schechter

Teapot Dome field is located 35 miles north of Casper, Wyoming in Natrona County. This field has been selected by the U.S. Department of Energy to implement a field-size CO_2 storage project. With a projected storage of 2.6 million tons of carbon dioxide a year under fully operational conditions in 2006, the multiple-partner Teapot Dome project could be one of the world's largest CO_2 storage sites.

CO_2 injection has been used for decades to improve oil recovery from depleted hydrocarbon reservoirs. In the CO_2 sequestration technique, the aim is to "co-optimize" CO_2 storage and oil recovery.

In order to achieve the goal of CO_2 sequestration, this study uses reservoir simulation to predict the amount of CO_2 that can be stored in the Tensleep Formation and the amount of oil that can be produced as a side benefit of CO_2 injection.

This research discusses the effects of using different reservoir fluid models from EOS regression and fracture permeability in dual porosity models on enhanced oil recovery and CO_2 storage in the Tensleep Formation. Oil and gas production behavior obtained from the fluid models were completely different.

Fully compositional and pseudo-miscible black oil fluid models were tested in a quarter of a five spot pattern. Compositional fluid model is more convenient for enhanced oil recovery evaluation.

Detailed reservoir characterization was performed to represent the complex characteristics of the reservoir. A 3D black oil reservoir simulation model was used to evaluate the effects of fractures in reservoir fluids production. Single porosity simulation model results were compared with those from the dual porosity model.

Based on the results obtained from each simulation model, it has been concluded that the pseudo-miscible model can not be used to represent the CO_2 injection process in Teapot Dome. Dual porosity models with variable fracture permeability provided a better reproduction of oil and water rates in the highly fractured Tensleep Formation.

DEDICATION

To

God, for being with me always.

To

My lovely wife, Laura, for her love, trust and continuous encouragement.

For being my best friend and the "soul out of my soul"

To

My happy, shining and creative daughters, Maria Fernanda and Maria Paula

My energetic, bright, boundless son, Juan Felipe

You keep my spirit alive!

To

My parents and all my family for their guidance, support, love and enthusiasm.

ACKNOWLEDGEMENTS

I would like to express my sincere gratitude to my research advisor, Dr. David S. Schechter, for assisting and supporting this research. His knowledge, support, and friendship have made my work possible and enjoyable.

I also wish to thank Dr. Daulat Mamora and Dr. Steven Dorobek for their advice and for serving as members of my graduate advisory committee.

I would like to extend my appreciation to Dr. Erwinsyah Putra for his guidance and support during the development of this research.

It has been a pleasure to work with all members of the brilliant Reservoir Management group: Deepak, Kim, Vivek, Matew and Zuher.

I would like to thank the professors and staff at the Department of Petroleum Engineering at Texas A&M University for all of their support.

Last, I wish to express my gratitude to the U.S. Department of Energy for sponsoring this study.

TABLE OF CONTENTS

Page

CHAPTER Page

LIST OF FIGURES

FIGURE Page

FIGURE Page

LIST OF TABLES

TABLE Page

CHAPTER I

INTRODUCTION

1.1 Background

Teapot Dome field, also known as Naval Petroleum Reserve #3 (NPR-3) is located in the southwest portion of the Powder River Basin, 35 miles north of Casper, Wyoming in the Natrona County (Figure 1.1). The reserve is a Government-owned oil field of 9,481 acres and was established in 1915 by executive order from President Wilson and became famous during the 1920' during the scandals of the Harding administration. The field is operated by the Department of Energy (DOE) through its Rocky Mountain Oilfield Testing Center (RMOTC).

Some activity occurred during a period of production in the 1920s and during 1958 to 1976 to mitigate loss of oil off the reserve. Full production was initiated in 1976 as provided by the Naval Petroleum Reserve production Act which mandates production of the reserve at the minimum efficient rate. Under the Act, production is authorized for 6 years and the U.S. President is authorized to extend production in increments of up to 3 years each. Each period the President makes his decision for extension on the basis that production, in contrast to shut-in, would produce revenue for the federal government and provide national security benefits.[1]

Oil production in Teapot Dome field is from three formations, the shallow Shannon Formation, at depths of 400 to 1000 ft; the Second Wall Creek member of the Frontier Formation at 2500 to 3000 ft; and the Tensleep Sandstone at 5500[2] ft. Teapot Dome gets its name from nearby Teapot Creek which in turn was named for Teapot Rock, 6 miles southwest of the structure.

This thesis follows the style of *SPE Reservoir Evaluation and Engineering*.

Teapot Dome is considered as an extension of the much larger Salt Creek anticline; an oil field operated by Anadarko Petroleum Co.

Primary depletion drive production of the Tensleep Formation began in 1978 with single well production rates no greater than 150 STBD

Teapot Dome field initially contained more than 5 million barrels of oil in the oil column (OC), which is the interval of the San Andres hydrocarbon accumulation above the producing oil/water contact (OWC). The field's producing oil water contact (POWC), above which oil is produced water-free during primary recovery is -400 ft below sea level. Tensleep Formation does not contain a primary gas cap.

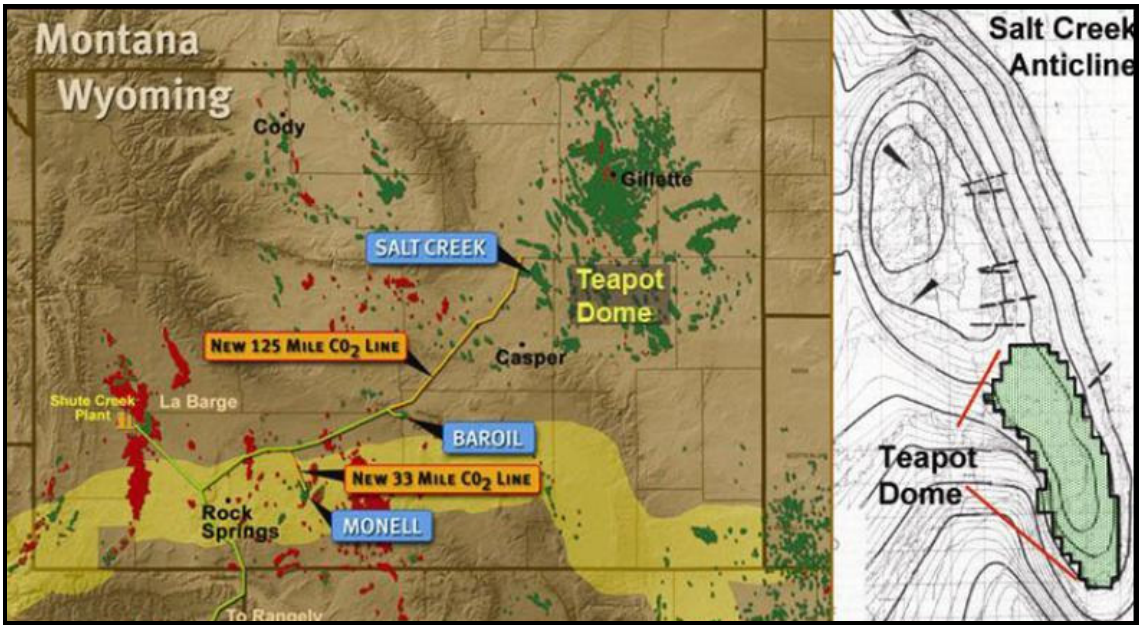

Figure 1.1 - Location map of Teapot Dome Field.

1.2 Problem Description

This research evaluates the effects of natural fractures and the hydrocarbon characterization in CO_2 storage process in the Tensleep Formation. Due to the presence of high permeability channels in the reservoir, the amount of CO_2 that can be injected varies across the field affecting the overall CO_2 storage goals in the project.

Tensleep reservoir fluid composition indicates dead oil characteristics. CO_2 injection and miscibility process response depends on how the reservoir oil has been characterized. Evaluation of different reservoir fluid models via reservoir simulation will provide additional evidence to establish the fluid model to be used in field scale CO_2 injection.

1.3 Objectives

The main objective of this research is establish the amount of CO_2 that can be storage and the additional oil that can be recovered from Tensleep Formation, Teapot Dome field by the CO2 injection process.

The specific objectives are to evaluate how fracture permeability and reservoir hydrocarbon model affects CO_2 injection process to "co-optimize" the CO_2 storage and enhanced oil recovery performance using single and dual porosity simulation models.

Fracture permeability will be incorporated from fracture aperture measurements in core samples using X-Ray Computer Tomography Scanner.

CHAPTER II

LITERATURE REVIEW

2.1 CO_2 Flooding Mechanisms

Carbon dioxide injection has been used in enhanced oil recovery (EOR) processes applicable to light to medium oil reservoirs since the 1970s; the traditional approach is oriented to recover the higher amount of oil from the reservoir injecting the minimum amount of gas.

There is a significant experience and knowledge in the oil industry to separate, transport, inject and process the quantities of CO_2 required in different projects.

The recovery mechanisms in immiscible processes involve reduction in oil viscosity, oil swelling, and dissolved-gas drive. CO_2 has a viscosity similar to miscible or light hydrocarbon components. Miscible displacement between crude oil and CO_2 is caused by extraction of hydrocarbons from the oil into the CO_2 and by dissolution of CO2 into the oil. In general, CO_2 is very soluble in crude oils at reservoir pressures swelling the oil and reducing its viscosity.[3]

Multiple-contact miscibility process governs the mixture between CO_2 and crude starting with CO_2 as a dense-phase and hydrocarbon liquid. CO_2 first condenses into the oil, making it lighter and extracting methane from the oil bank. The lighter components of the oil then vaporize into the CO_2-rich phase, making it denser, more like the oil, and thus more easily soluble in the oil. Mass transfer continues between the CO_2 and the oil until the two mixtures become indistinguishable in terms of fluid properties. Figure 2.1 illustrates the condensing/vaporizing mechanisms for miscibility.[4]

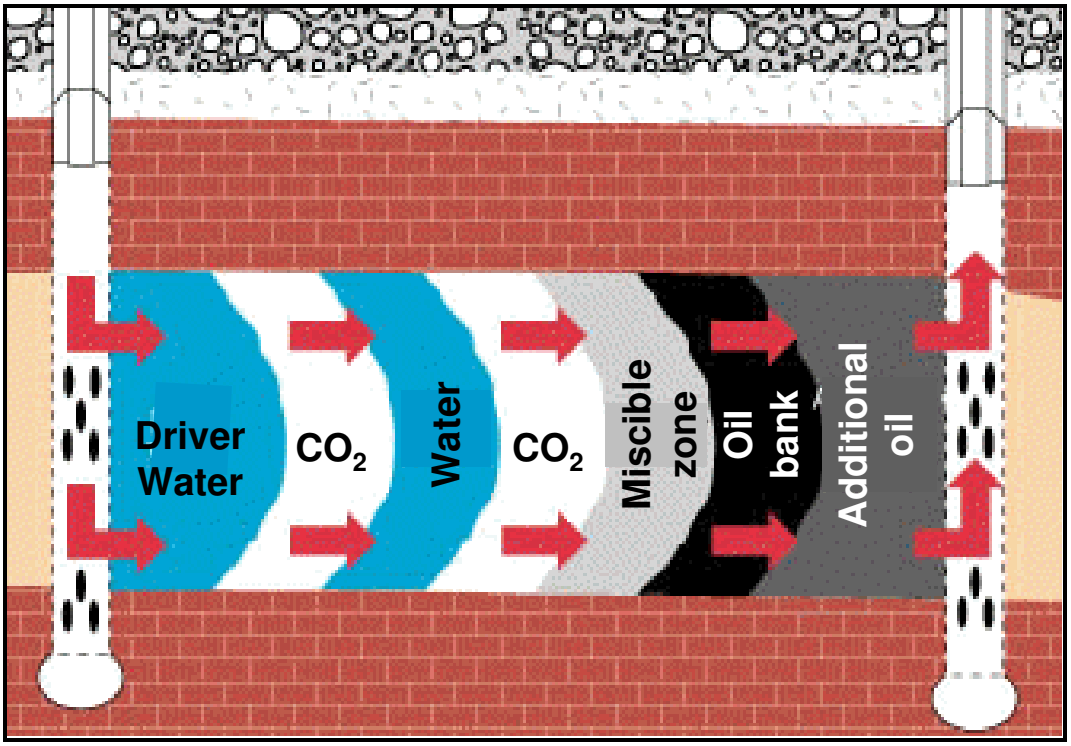

Figure 2.1 - One-dimensional schematic showing CO_2 flooding.[4]

Because of this mechanism, oil recovery may occur at pressures high enough to achieve miscibility. CO_2 needs to be compressed at high pressures to reach a density at which it becomes a solvent for the lighter hydrocarbons in the crude oil. This pressure is known as "minimum miscibility pressure" (MMP) and it is the minimum pressure at which miscibility between CO_2 and crude oil can occur.[3]

2.2 CO_2 Storage

The CO_2 storage from the flu gases did not start because environmental concerns about green house effect, instead, it gained attention as a source for enhance oil recovery processes. It is very likely that fossil fuels will be the main source of energy in the 21 st century. However increased concentrations of carbon dioxide due to carbon emissions are expected.

CO_2 has been actively injected into geological formations, oil and gas reservoirs, unmineable coal seams and deep saline reservoirs (Figure 2.2). These formations have storage oil, natural gas, brine and CO_2 over million of years proving to be effective seals. These seals maintain their integrity as long as the original pressure of the reservoir is not exceeded. Monitoring and verification of CO_2 flow in geological formations is critical for gas sequestration, but technical development is in its infancy.[5]

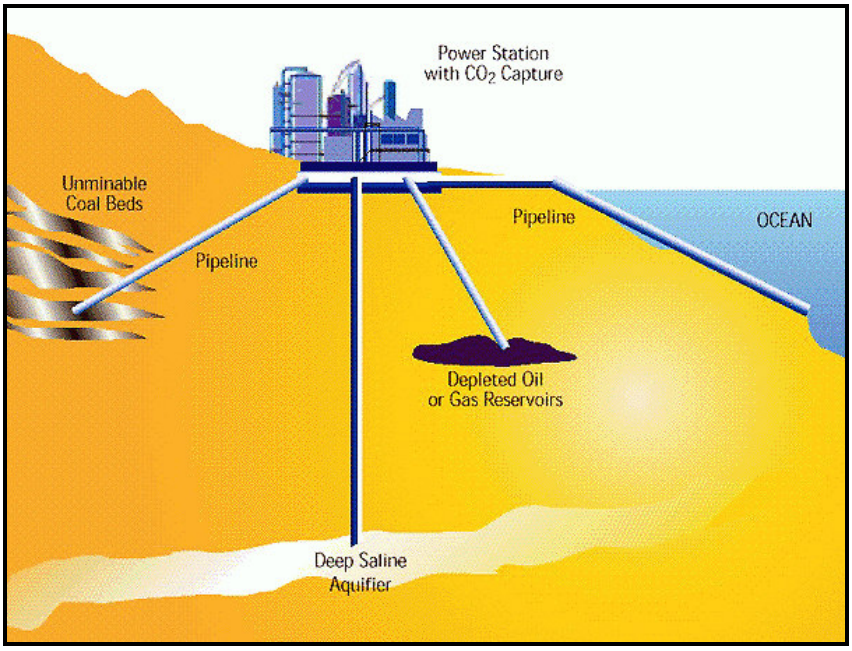

Figure 2.2 - CO_2 geological storage.[6]

Hydrocarbon production from oil and gas reservoirs can be enhanced by pumping CO_2 gas into the reservoir. This process represents an opportunity to store carbon at a low cost due to the revenues from oil and gas recovery. The United States is the world leader in enhanced oil recovery technology, using about 32 million tons of CO_2 per year for this purpose.

Coal beds typically contain large amounts of methane adsorbed onto the surface of the coal. The current practices to recover the methane are depressurizing the coal bed or inject CO_2. CO_2 have twice the methane adsorption rate and tend to remain storage in the carbon bed.[7] Methane provides a value-added revenue stream to the carbon storage process.

Saline formations do not provide products economically exploitable when carbon is storage, but it has other advantages. The storage capacity of saline formations in United States has been estimated at up to 500 billion tones of CO_2 and carbon sources are within easy access to saline injection points.

Before CO_2 can be stored, it must be captured as a relatively pure gas. In the United States, however, CO_2 is routinely separated and captured as a by-product from industrial processes. Usually power plants exhaust CO_2 diluted with nitrogen as flue gas. Commonly coal-fired power plant flue gas contains 10-12 % of CO_2 by volume and from natural gas plants between 3-6 %. Existing capture technologies are not cost-effective when considered in the context of CO_2 storage from power plants.

Good oil response, gas injectivity and gas production within designed limits are considered as positives aspects from the CO_2 injection process. Simultaneously one of the main concerns in the projects performed has been the early CO_2 breakthrough, which compromises gas processing facilities.

2.3 Parameters Affecting a CO_2 Storage Process

2.3.1 Reservoir Heterogeneity

Reservoir heterogeneity has a strong influence on the gas/oil displacement process.[8] The degree of vertical reservoir heterogeneity can affect the CO_2 performance. Formations with higher vertical permeability such as naturally fractured reservoirs are influenced by

cross-flow perpendicular to the bulk flow direction.[9] Cross-flow is more commonly presented in water alternate gas (WAG) projects, this may increase the vertical sweep but generally the oil recovery is low due to the gravity segregation and decreased flood velocity in the reservoir, Figure 2.3. As CO_2 flows preferentially toward the top portion of thick, high permeability zone, injected water may flow preferentially toward the lower portion of the zone.

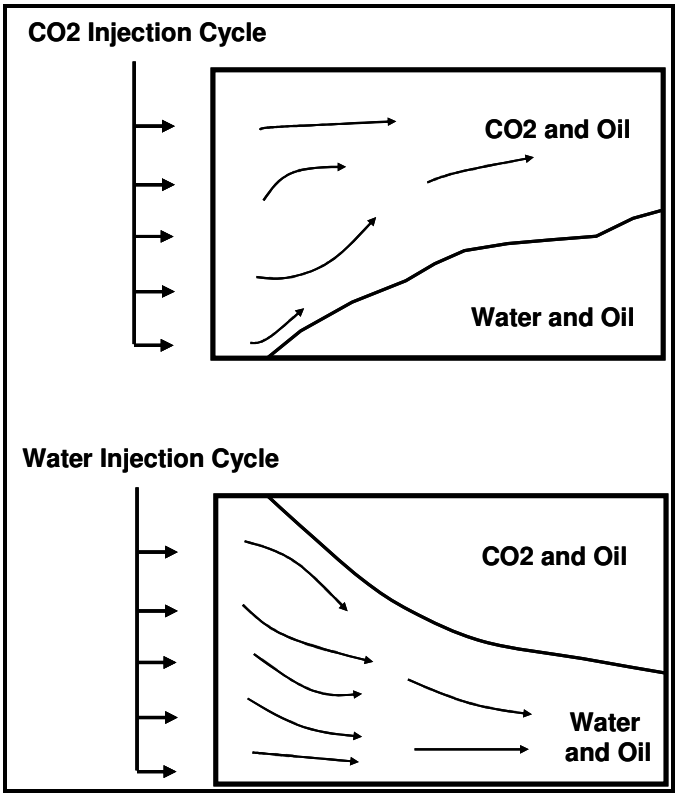

Figure 2.3 - Effect of gravity during WAG injection.[4]

2.3.1.1 Relative Permeabilities

As an important petrophysical parameter, relative permeability includes rock wetting characteristics, heterogeneity of reservoir fluids and rock and fluid saturations. Relative

permeability commonly changes during alternate water/CO_2 injection, water injectivity is significantly reduced after the first gas injection cycle due to the effect of CO_2 on water relative permeability. It is very important to have a good understanding of the relative permeability curves to be used in reservoir simulators to predict the CO_2 storage.[4]

Laboratory experiments have showed hysteresis effects in the water relative permeability between the drainage and imbibition curves. Irreducible water saturations after drainage cycles were 15 to 20% higher than the initial connate water saturation.[10]

Hysteresis refers to the directional saturation phenomena exhibited by many relative permeability and capillary pressure curves when a given fluid phase saturation is increased or decreased.[11] This phenomena is illustrated in Figure 2.4.

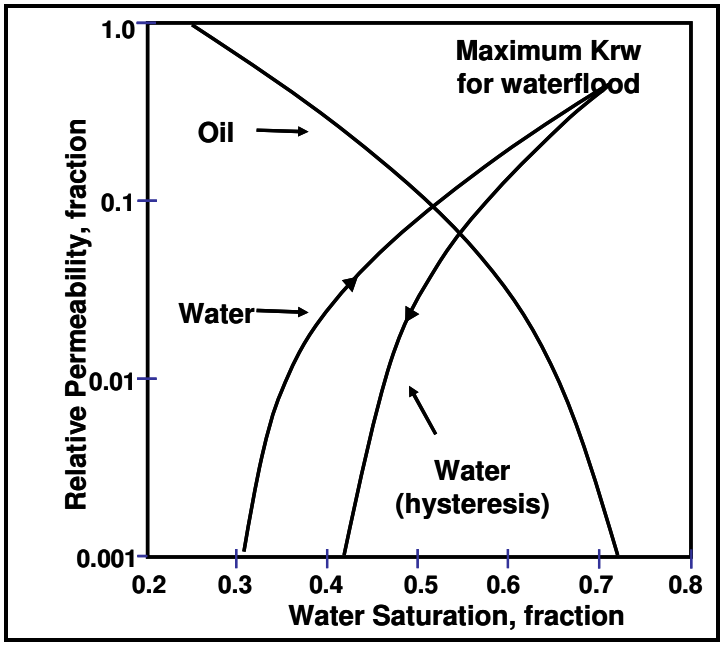

Figure 2.4 - Two-phase relative permeability diagram.[7]

2.3.1.2 Natural Fractures

Structures such as fractures, fracture networks, and faults can influence permeability and therefore fluid flow within an aquifer or petroleum reservoir. Distinct permeability anisotropy has been observed in reservoirs with low matrix permeability and a well developed open fracture systems, with the highest permeability parallel to the fractures. Within a given rock volume, fractures generally result in an overall permeability increase. Significant interaction between the fracture surface and the matrix allows better drainage of the rock matrix. This matrix/fracture interaction could allow for a substantial increase in recoverable hydrocarbon reserves.

In contrast, mineralized fractures and deformation bands (i.e., small displacement faults characterized by tight cataclasis and/or pore reduction through compaction) are typically characterized by significant permeability reduction. Where fractures are mineralized or the rock is cut by deformation bands, the rock matrix is more permeable than the structures, so the rock is more permeable parallel to, and between, fractures and deformation bands. Therefore, within a given rock volume containing mineralized fractures and/or deformation bands, there will be overall permeability decrease and possible reservoir compartmentalization. Partially mineralized fractures may still have some permeability. However, there could be a significant reduction in the interaction between the remaining open fracture fluid pathway and the rock matrix. Either mineralized or partially mineralized fractures could have the effect of decreasing the total amount of recoverable reserves.

Fractures commonly increase or decrease permeability in certain directions and thus introduce permeability anisotropy and heterogeneity; and it is important, from a production standpoint, that they can be modeled accurately. It can be very difficult, however, to predict the location, spacing and orientation of fractures and small-displacement faults in the subsurface. Most regional fractures are sub-vertical, and are thus unlikely to be sampled in vertical boreholes. Reasonable predictions of

permeability anisotropy require an understanding of controls on the distribution and orientations of such features. Fractures can have predictable orientations with regard to large-scale structures such as anticlines.

For modeling and production purposes, it is important to document directions of preferred fracture and fault orientations within primary hydrocarbon traps, such as anticlines. By understanding controls on fracture and fault orientation and distribution in a given reservoir, the accuracy of flow modeling can be improved, thereby increasing primary and secondary hydrocarbon recovery.[12]

2.3.2 Reservoir Fluids

Reservoir fluid composition controls the miscible process between the reservoir fluid and injected CO_2. CO_2 is less dense and viscous than reservoir fluids

Complete dissolution of injected CO_2 takes place in a scale of hundred to thousand of years, this depending on the gas migration and fluids reaction.[13]

When reservoir characterization is well understood and described, CO_2 injection process has performed as expected.

As carbon dioxide CO_2 is injected in the formation, it mobilizes oil, dissolves into brine and promotes dissolution of carbonates cements.[14] Brine can become supersaturated with dissolved solids and when pressure drops as it advances through the reservoir, precipitates such as gypsum can form.[5]

CHAPTER III

GEOLOGY REVIEW

3.1 Introduction

Teapot Dome also known as the Naval Petroleum Reserve No. 3 (NPR-3) is located in central Wyoming, near the southwestern edge of the Powder River Basin, (Figure 3.1). The deepest portions of the Powder River Basin contain nearly 5,500 m of sedimentary rocks, approximately 2,440 m of which are non-marine, Upper Cretaceous and lower Tertiary clastic sedimentary rocks related to Laramide orogenesis (Fox *et al*., 1991).[12] The structural style is represented mainly by basement-involved tectonic structures, associated with the Laramide orogeny. The greatest deformation is concentrated along the western and southern structure margins.

Teapot Dome is one of several productive structural hydrocarbon traps associated with Laramide structures in this area. It is part of a larger structural complex which comprises the Salt Creek anticline to the north and the Sage Spring Creek and Cole Creek oil fields to the south (Doelger *et al*., 1993; Gay, 1999).[12] Teapot Dome is also similar to other Laramide structures such as Elk Basin anticline and Oil Mountain (Engelder *et al*., 1997; Hennings *et al*., 1998; Hennings *et al*., 2000).[12]

Teapot Dome is a basement-cored anticline, similar to other structures within the Rocky Mountain region that have been hydrocarbon exploration targets since the turn of the past century. Structures of this type can be found in many other areas of the world (e.g., DeSitter, 1964; Harding and Lowell, 1979).[12]

Teapot Dome field is a large northwest-southeast trending anticline considered as an extension of the larger Salt Creek anticline. It is a double plunging structure with four-

way closure, asymmetrical and SW verging; limited on its west flank by a large regional fault.

One of the primary reasons basement-cored anticlines are exploration targets is that they can provide excellent four-way closure. Four-way closure can allow the entrapment of migrating hydrocarbons in economically significant amounts. To maximize recovery of these trapped hydrocarbons, it is essential to accurately model any permeability anisotropy associated with these structures.

A total of nine (9) productive horizons (Figure 3.2) including the shales of Shannon, Steele and Niobara formations are present, Second Wall Creek and Tensleep sandstone formations being the most productive. Tensleep is the lowest producing formation found in Teapot Dome and is generally found at the bottom of each well, which complicates the formation evaluation as the layer is not completely logged.[15]

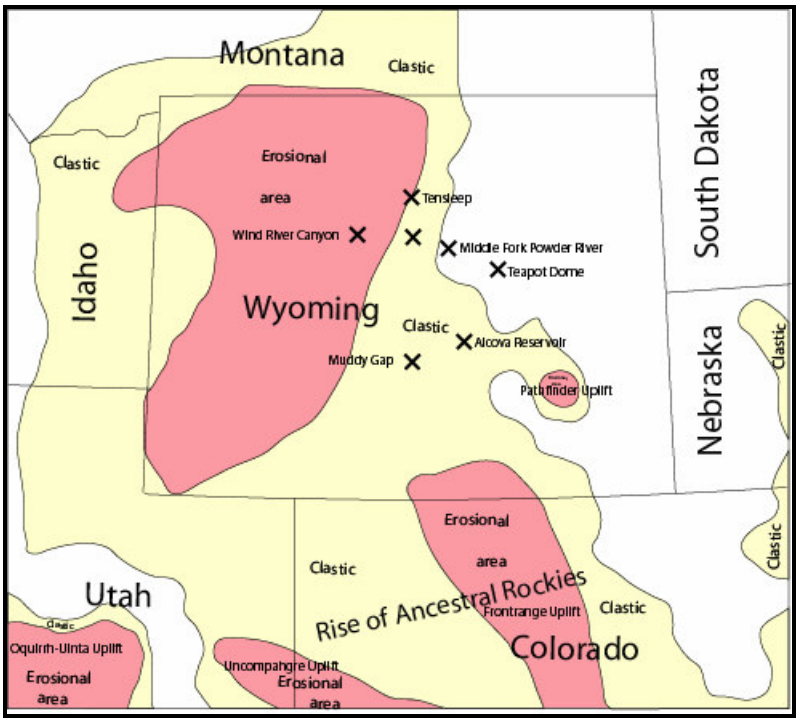

Figure 3.1 - Location of Teapot Dome Field in the Permian Basin.[17]

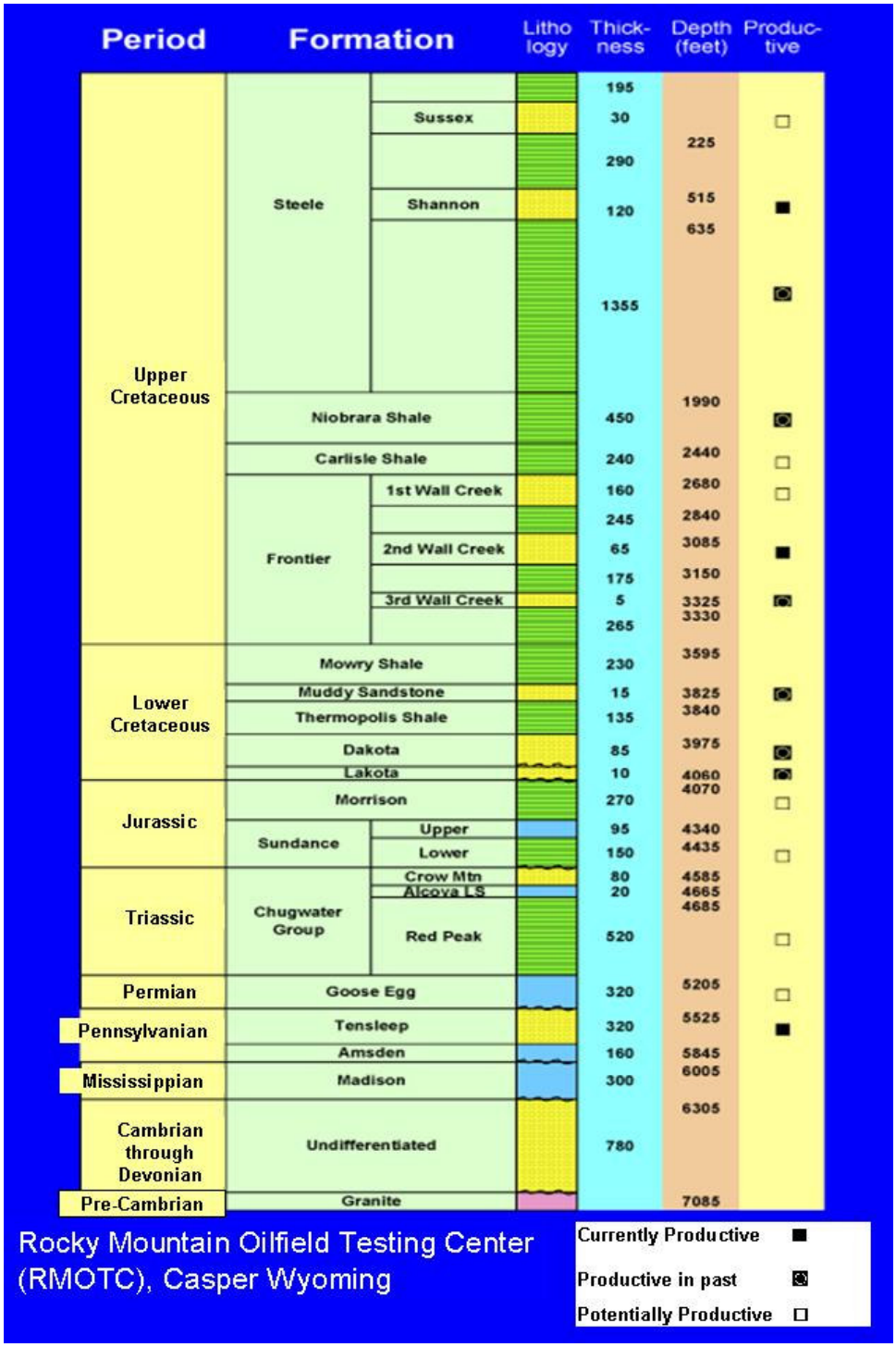

Figure 3.2 - Generalized stratigraphic column showing Permian section at the Teapot Dome field.[16]

3.2 Stratigraphy and Depositional Environment

The Tensleep Formation of Pennsylvanian age consists of 300 ft of multi-sequence boundaries between sandstone and dolomite, is the deeper formation in Teapot Dome field and an important producing unit elsewhere in Wyoming. Stratigraphicaly, it is located between dolomite strata of the Goose Egg Formation, which is not productive in the Teapot Dome area although it may have some potential not evaluated, and dolomite units of the underlying Amsden Formation, Figure 3.3.

Tensleep sandstones contain multiple sequence boundaries in response to frequent and high-amplitude sea level changes. Thin dolomites relatively continuous cap each dune deposition sequence.

Generally from bottom to top, Tensleep sandstone changes from dominantly marine, with abundant crinoids and corals, thick tabular carbonate beds and thin sandstone layers, to dominantly continental, with thick eolian cross-bedded sandstones, scarce fossils, and thin and discontinuous carbonates.[17]

The Tensleep Formation is hard and tight, regionally located where good sandstones on the west change eastward to dolomitic limestones, anhydrites and thin sandstones of the Minnelusa facies.[2] Clay is rare and less than 1% (1'/100').

Cementation by dolomite, calcite, anhydrite and quartz has greatly reduced porosity and permeability in the Tensleep sandstone, whereas dissolution of cements during diagenesis has enhanced both porosity and permeability.[17]

An evaluation of gamma ray, resistivity, bulk density, compression and acoustic impedance logs from Well 11-MX-11 were performed by RMOTC on January 2002. This evaluation provides the current stratigraphical division of the Tensleep Formation. This representation of so called flow units would honor the heterogeneity and zonation of the formation, (Figure 3.4).

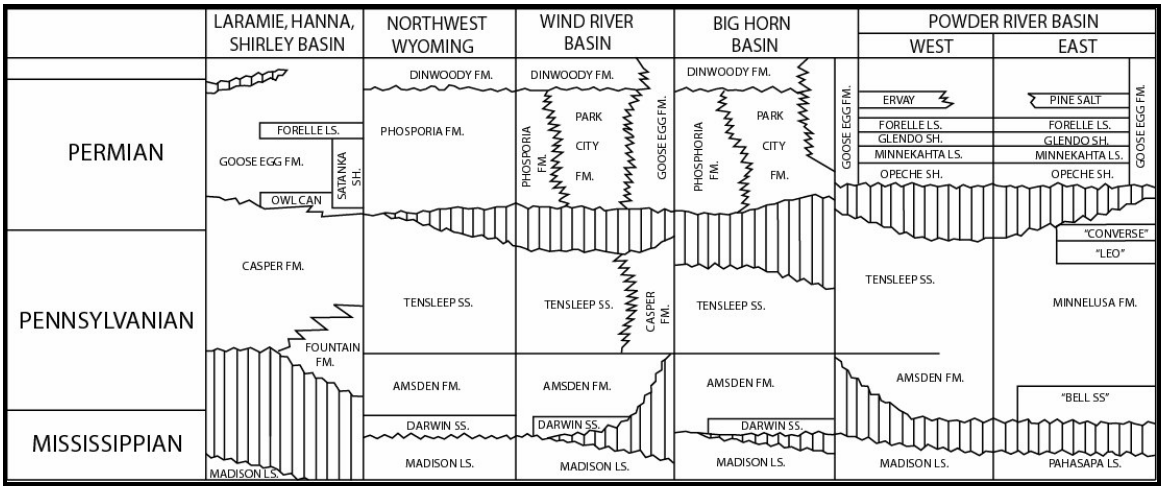

Figure 3.3 - Late Paleozoic stratigraphic chart of part of Wyoming.[17]

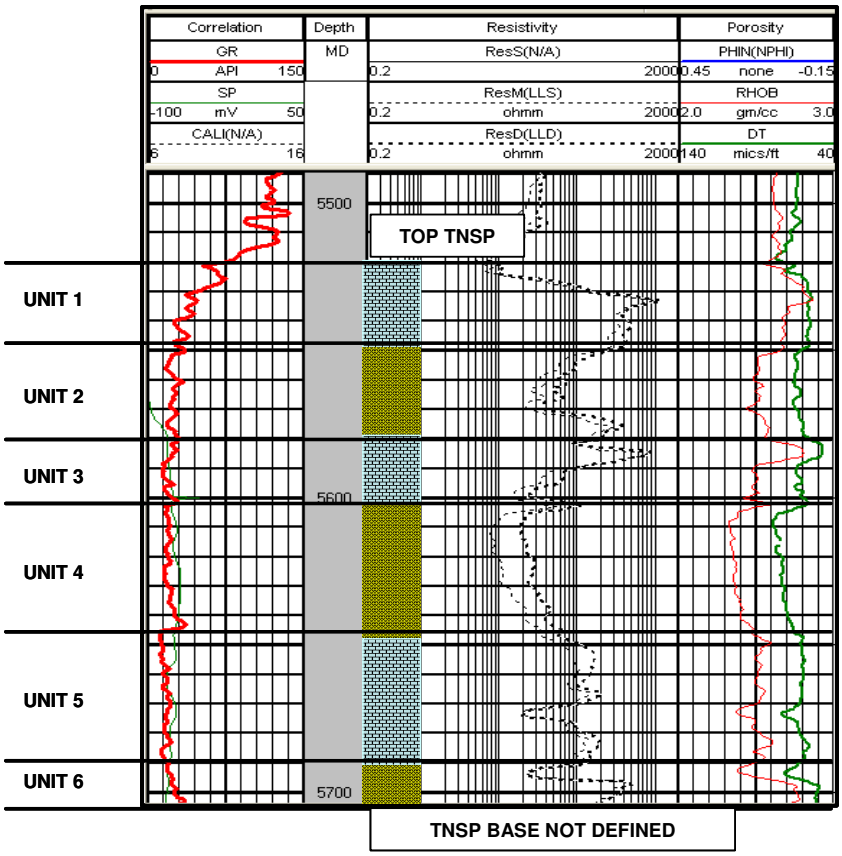

Figure 3.4 - Tensleep Formation type log well 11-MX-11.

3.3 Seismic Interpretation

A 3D seismic survey designed to image the Pennsylvanian Tensleep Formation was shot in the field on January 2001, with a coverage of 72.3 square kilometers (17800) consisting of 345 in-lines and 188 cross-lines with a bin size of 110 ft. 38 km^2 was available for interpretation. This 3D seismic information covers the Teapot Dome structure completely as shown in Figure 3.5.

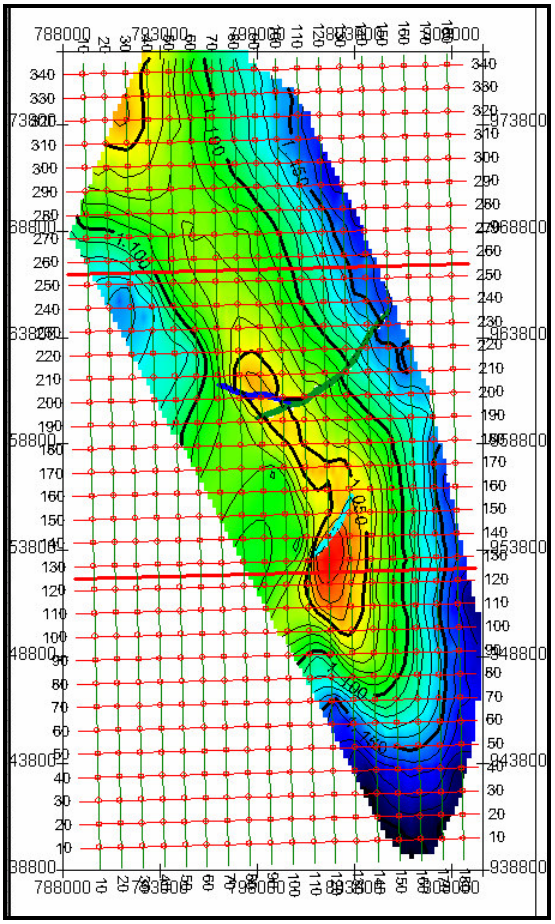

Figure 3.5 – Time map showing seismic coverage at Tensleep Formation.

From a gravity survey view point, the basement rock, referred to as granite, will be approximately 750 feet closer to the surface at the top of the anticline than at the edges. The density contrast in the overlying formations is essentially the intrusion of the higher density granite basement as compared with the marine shales and sandstones of the producing formations.[15]

3.3.1 Time Interpretation

A post-stack migrated volume acquired on January 2001 was interpreted in time. Well log information and geological tops measured in Well 62-X-11 were used to generate a velocity log and a synthetic seismogram (Figure 3.6). This well provides useful information to assist with the interpretation. The synthetic seismogram allowed the identification of a dolomite marker at the top of Tensleep Formation (TNSP) (Figure 3.7). This marker has good seismic continuity in the area of interpretation.

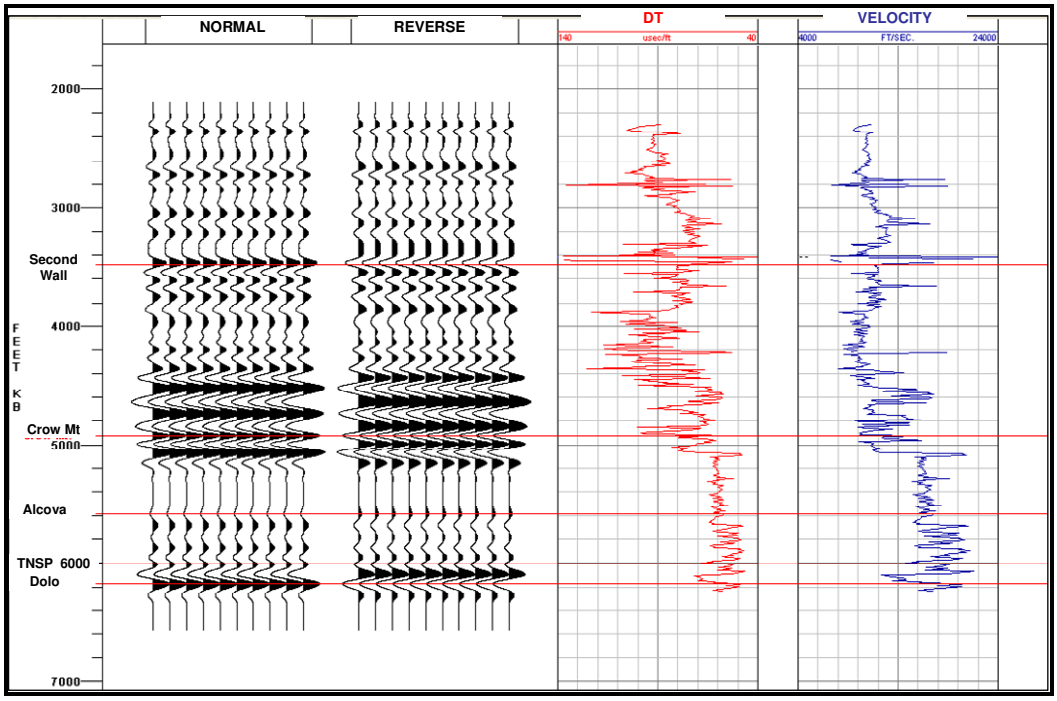

Figure 3.6 - Seismogram log from well 62-X-11.

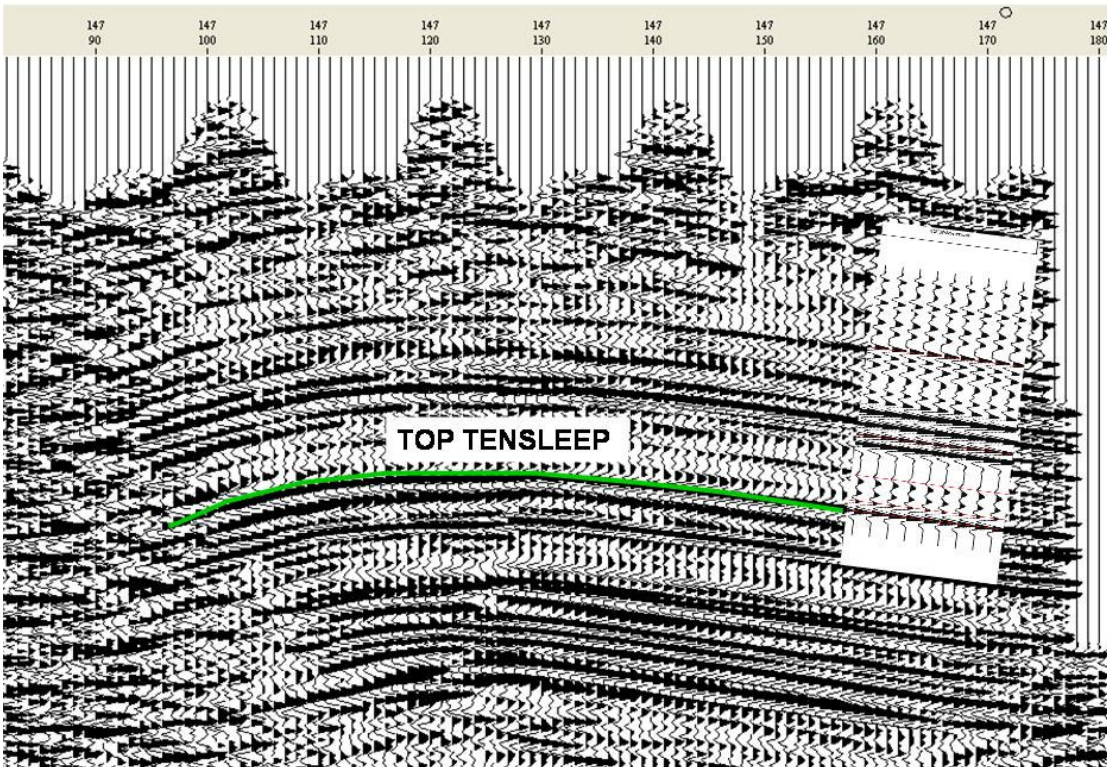

Figure 3.7 - Synthetic seismogram from well 62-X-11.

The interpretation of the dolomite marker provided a top isochron map that indicates a semi-regular spaced northeast-southwest trending fault system cutting the horizon with major faults approximately every mile.

The main fault (MF1) is a reverse fault that strikes NW-SE, and is considered to be the west limit of the field, A second system of normal faults with N45E direction is present, where fault 3 (F3) divides the Tensleep structure in Teapot Dome field from Salt Creek field, Figure 3.8.

A third strike fault (SF) located south of fault F3 is at crest of the structure. This area can be considered of good productivity because most of the wells are located near this fault, (Figure 3.9). The Final isochron map at top of Tensleep Formation can be observed in Figure 3.10.

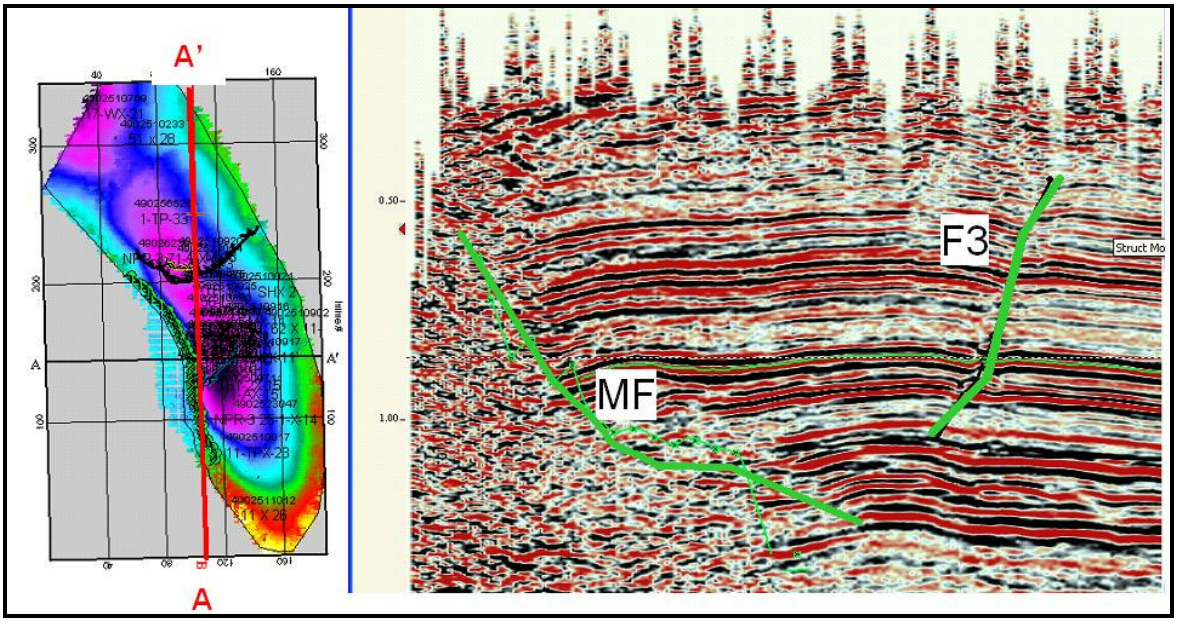

Figure 3.8 - Cross line A-A'.

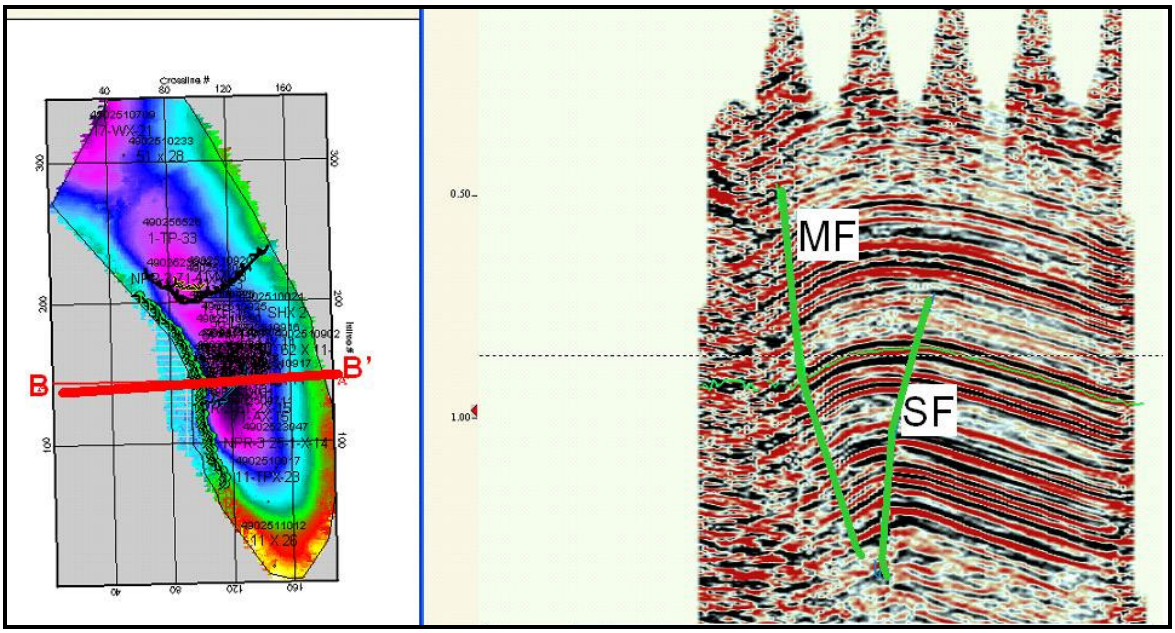

Figure 3.9 - Inline B-B'.

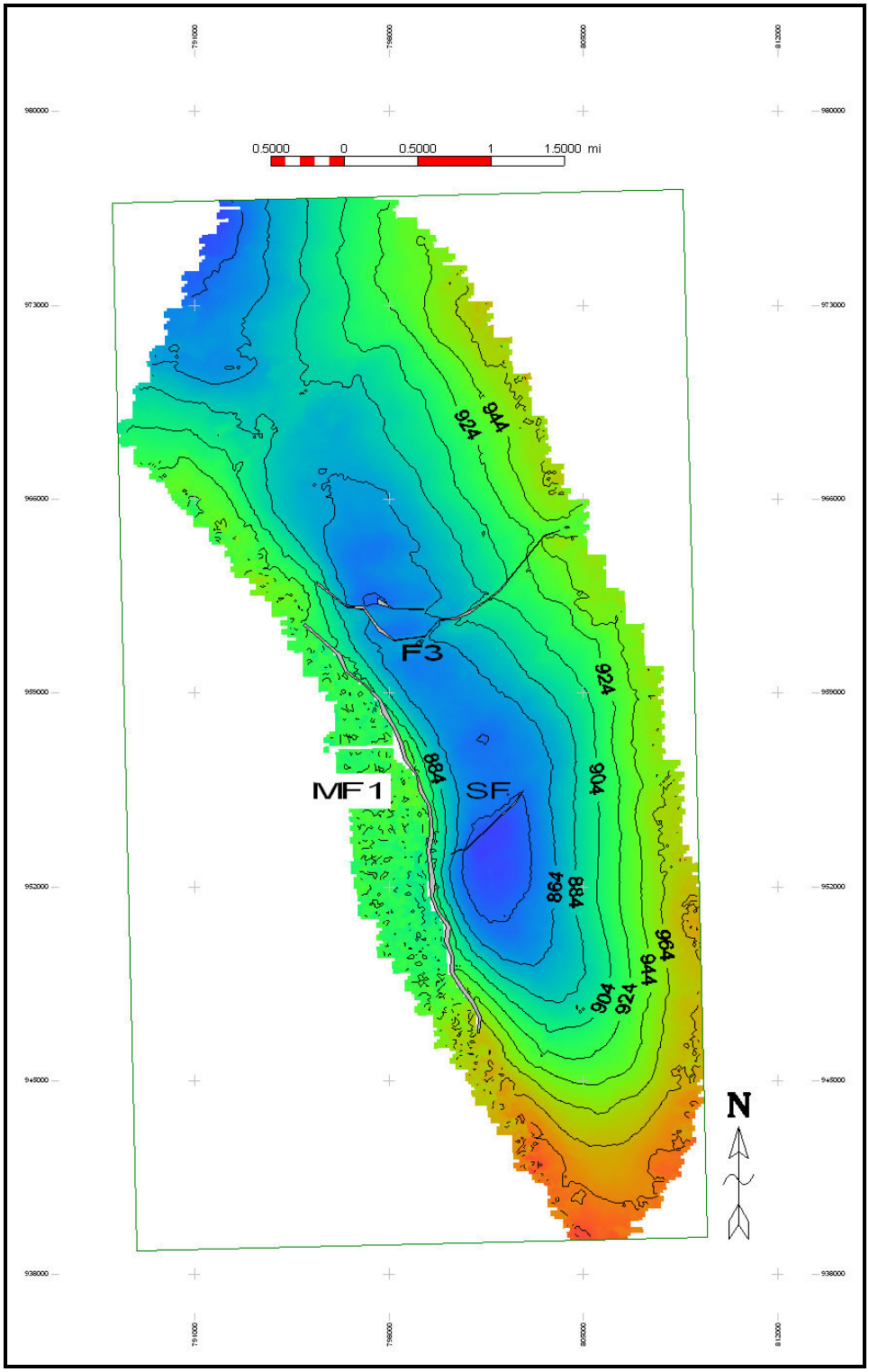

Figure 3.10 - Isochron Map for Tensleep Formation at Teapot Dome.

3.3.2 Time to Depth Conversion

A structural map at the top of the Tensleep Formation was generated by integrating seismic time interpretation and well depths information, (Figure 3.11). The conversion was done by the multiplication of the isochron grid with the average velocity or pseudo-velocity grid. The pseudo-velocity map came from the Tensleep depth in the wells and the time in the isochron map, this velocity is in agreement with the velocity calculated from the sonic log.

No check shots or vertical seismic profiles (VSP) data have been taken in the field. An average of 4267 m/sec was used to generate a projection from the time surface into elevation map.

The structural map has the sub sea level as reference and it was weighted with the well tops information in the field.

3.4 Fracture Evaluation from Cores

About 197 ft of core was recovered from the Tensleep Formation from the well RMOTC 48-TPX-28 in May of 2004. The core was relatively broken in the coring process especially in the intervals containing numerous natural fractures. High fracture intensity is reported in a core description performed in the Sandia National Laboratories, (Figure 3.12).

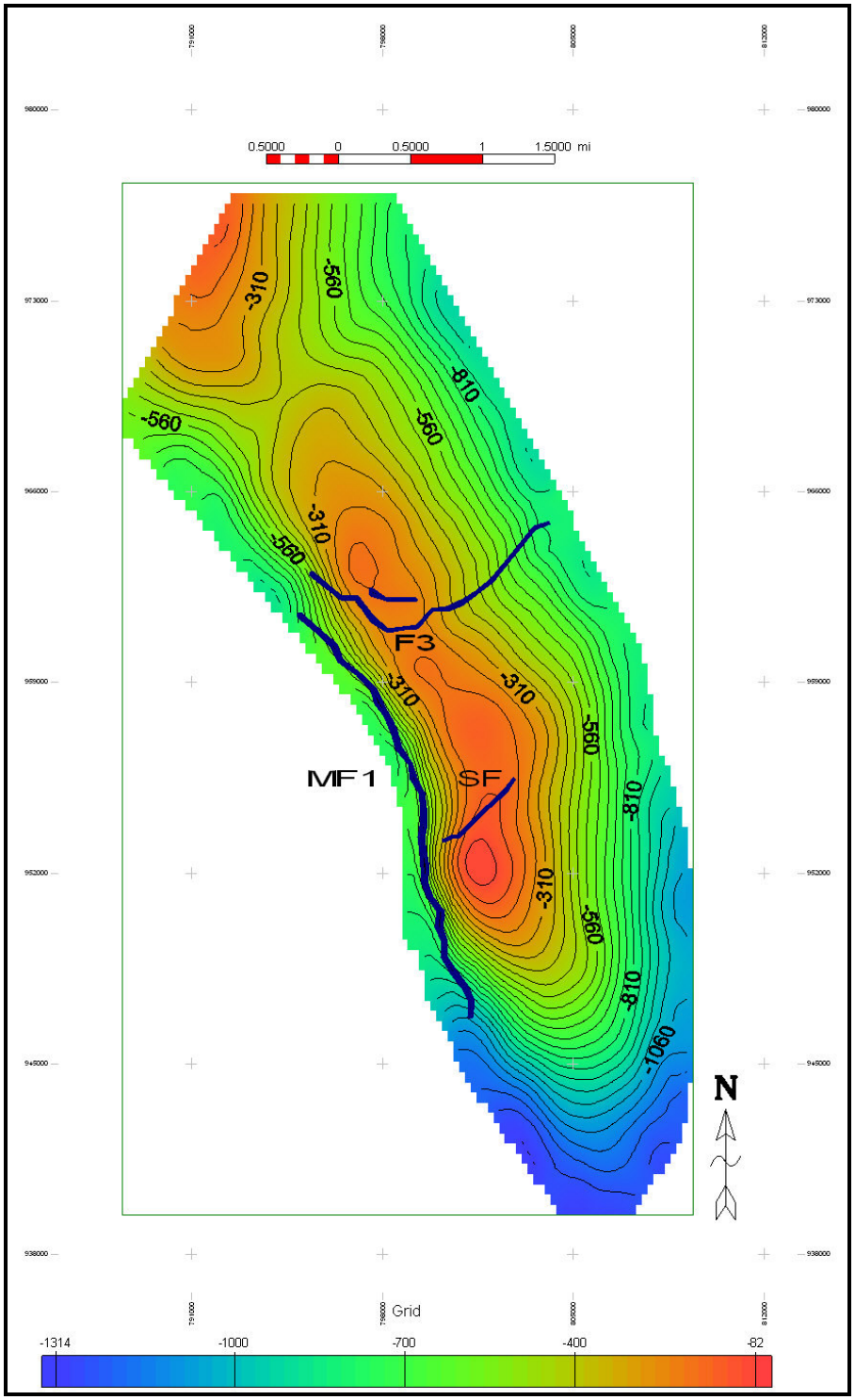

Figure 3.11- Structural Map for Tensleep Formation.

Figure 3.12- Highly fractured Tensleep sandstone.

Fractures are present in both, sandstone and dolomites. Fracture intensity can be measure as one fracture per ten feet of core. Fractures are mostly vertical to near-vertical and commonly terminate at bedding planes and stylolites, although many of them terminate within upper layers.

Most of the fractures present an aperture less than one millimeter (1 mm) in total width. The aperture is occluded in the small fractures by partial mineralization of quartz and/or dolomite, (Figure 3.13). Significant porosity remains in the fractures between 10 to 18 %, especially in the large ones that usually splits the rock showing this mineralization as an incomplete and weak seal between fracture faces.

Figure 3.13- Natural fracture face partially covered with crystalline dolomite.

Some parallel and intersecting fractures were found in fine-grained dolomites where one of them was filled with dolomite in a 70% to 80%.

Bitumen lined fractures was observed in the fine-grained, white dolomite facies that overlies oil-stained reservoir sandstone.

A zone of inclined fractures, possibly a conjugated shear system is very similar to that seen in Tensleep outcrops at south of Alcova reservoir. FMI log indicates that the maximum horizontal in-situ compressive stress and most of the natural fractures strike E-W to WNW-ESE.

High degree of fracture connectivity supported by past pressure interference tests is present. A pump-off operations of a Tensleep completion, was felt impacted by operational swings in high volume Salt Creek field Tensleep producers.[18]

3.5 Lithologic Controls

Both fracture spacing and orientation vary with lithology at Teapot Dome. In general, fractures are most closely spaced in carbonaceous shales (Unit 4), more widely spaced in fluvial (Unit 5) and beach (Unit 2) sands, and most widely spaced in marine shales (Unit 1). Fractures are generally absent, replaced by deformation bands; within the white beach sandstones of Unit 3.[18]

CHAPTER IV

RESERVOIR PERFORMANCE

4.1 Reservoir Basic Data

Teapot Dome Field is considered as the continuation of the Salt Lake Field operated by Anadarko Petroleum Company. Teapot Dome produces light and sweet (low sulfur content, 0.16 %) oil from nine different formations. Just Tensleep Formation produces a lower gravity, sulfurous oil. This oil is mainly used for oiling roads and other lease uses. Tensleep the lower productive unit is located at subsea depths approximately at 5500 feet (5000 ft-ss).

Tensleep Formation is Pennsylvanian dolomite cemented sandstone with a gross thickness that varies between 250 and 300 ft. A net oil pay thickness about 75 feet has been measured from logs. It has been estimated that Tensleep Formation initially contains nearly 4.5 million barrels of oil in place. Hydrocarbon is accumulated between the high structural point at 80 ft-ss and the producing oil/water contact (OWC) estimated at 400 ft-ss.

No pressure data have been recorded in the formation, water production rates indicates that underlying formations are influenced by a strong aquifer. The aquifer has maintained almost constant reservoir pressure during the course of the field life. The pressure drop is less than 100 psi through out the Tensleep Formation. Water drive then considered as the primary producing mechanism in the reservoir. Table 4.1 summarizes basic reservoir and fluid data.

Table 4.1 - Summary of reservoir data.

Reservoir Characteristics	Values
Producing area	440 acres
Formation	Pennsylvanian Dolomitic Tensleep
Average Depth	5500 ft
Gas-oil Contact	No present
Average Matrix Permeability	80 mD
Average Porosity	13.50%
Oil Gravity	31 °API
Reservoir Temperature	190 °F
Primary production mechanism	Water Drive
Original reservoir pressure	2300 psi
Bubble point pressure	40-70 psi
Average pressure at start of CO_2 injection	2000± 100 psi
Initial FVF	1.312 RB/BBL
Solution GOR at original pressure	4 SCF/BBL
Oil viscosity at 60° F and 42 psi	3.5 cp
Minimum miscibility pressure	1300 psi

4.2 Reservoir Development History

Teapot Dome field had its first production from the so-called “Dutch” well with 200 BOPD from First Wall Creek sandstone in 1908. In 1909 a few wells value were drilled to develop the Shannon sand.

Prior to initiating the development and exploration program at Teapot Dome in 1976, 233 wells were drilled in all the producing formations. At 1996 additional 1007 development wells and 90 exploratory wells were drilled. 27 of the 1007 wells were drilled in fiscal year 1996 targeting Tensleep Formation. Two of these wells experienced the highest initial production rates of any wells in Wyoming at that time paying for their capital cost in less than 3 months.

Primary depletion began on 1977 when six wells were drilled in Tensleep Formation, however just one the structurally highest is capable of production (Well 74-CMX-10) with intermittent rates lower than 10 BOPD.[2]

Historical oil and water production from Tensleep Formation can be observed in Figure 4.1.

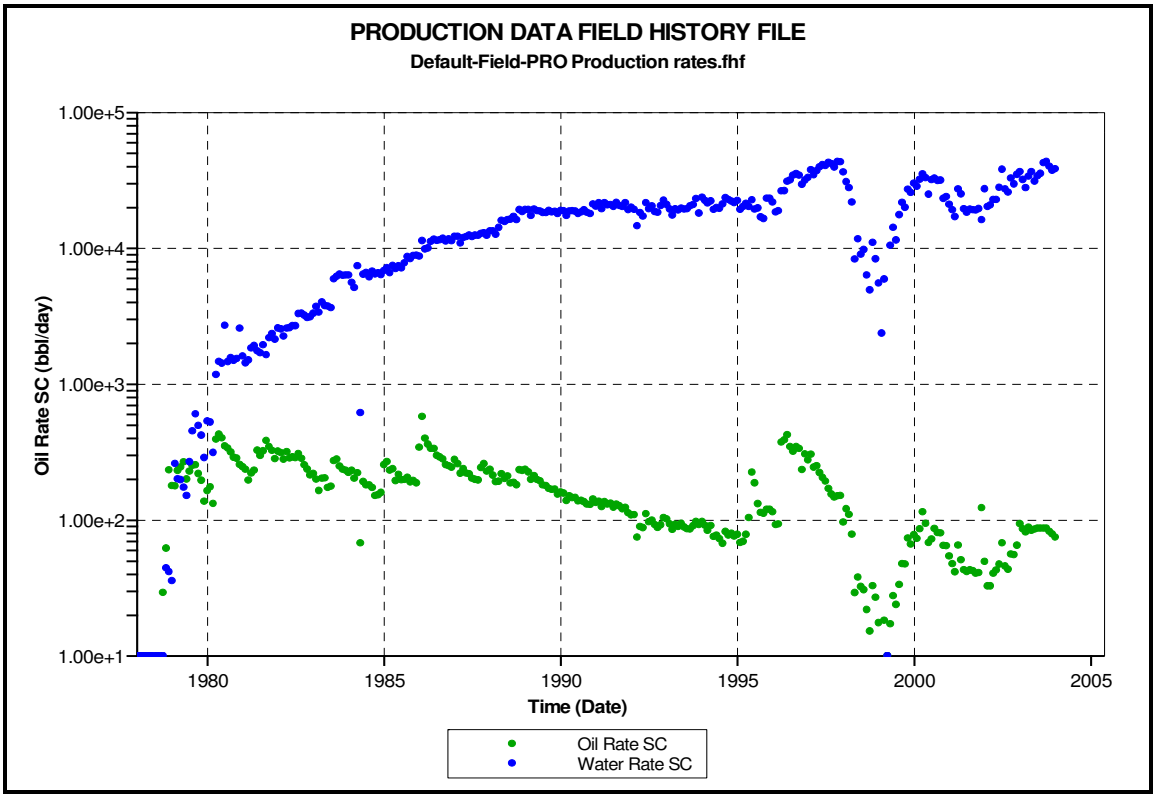

Figure 4.1 - Tensleep Formation production history.

CHAPTER V

SIMULATION PARAMETERS AND MODEL

All the reservoir parameters used in the simulation model are described in this chapter. Evaluation and definition of rock properties to be used in reservoir simulation is presented. Matrix and fractures relative permeabilities and capillary pressure data from Tensleep cores were defined. Matrix wettability and fracture spacing is established.

Calibration of equation-of-state to describe phase behavior of the reservoir fluid was obtained. Evaluation of compositional Vs pseudo-miscible approach is presented. The number of components in the fluid sample and component lumping process were compared to obtain the best fluid model in terms of accuracy in laboratory data reproduction and efficiency in simulation run time.

The initialization of the simulation model was conducted to assess the volume of the original hydrocarbon in place.

5.1 Numerical Simulator

One of the concerns about the reservoir fluid model was to select the simulator that best represents CO_2 displacement process. Compositional simulation and pseudo-miscible black oil models have been widely used to reproduce CO_2 displacement processes. The compositional simulators GEM™ [19] and, the black oil finite-difference simulator IMEX™ [20] were used in this study.

One compositional and one pseudo-miscible model were built to evaluate the accuracy of the black to represent CO_2 displacement process. Compositional simulation use equations of state (EOS) with theoretical parameters that are able to predict fluid behavior of hydrocarbon mixtures commonly encountered in oil and gas reservoirs.

Pseudo-miscibility simulator is a black oil approximation that takes into account only the gas dissolution.

Compositional model construction is time consuming and expensive. Pseudo-miscible option is capable of modeling the essential features of miscible displacement while leaving the fine structure of unstable miscible flow unresolved, making it possible to represent the reservoir by a fairly coarse numerical grid.[21]

5.2 Relative Permeability

5.2.1 Matrix Relative Permeability

Four rock samples were used in relative permeability laboratory tests. One sample A from 62-TPX-10 well (5443') and three samples from 43-TPX-10 well; sample B (5486'), sample C (5492') and sample D (5500'). The tests were performed using simulated reservoir brine and mineral oil with a viscosity of 30 cp.

Similar rock compositions have been encountered in the samples, sandstones with fine to very fine grains and well indurate are basic characteristics. Despite the similar composition, relative permeability experiments show important differences in the end-points. Initial water saturations (Swi) are between 12.5% to 22.1 and residual oil saturations (Sro) are between 28.7% and 56.3%, Figure 5.1.

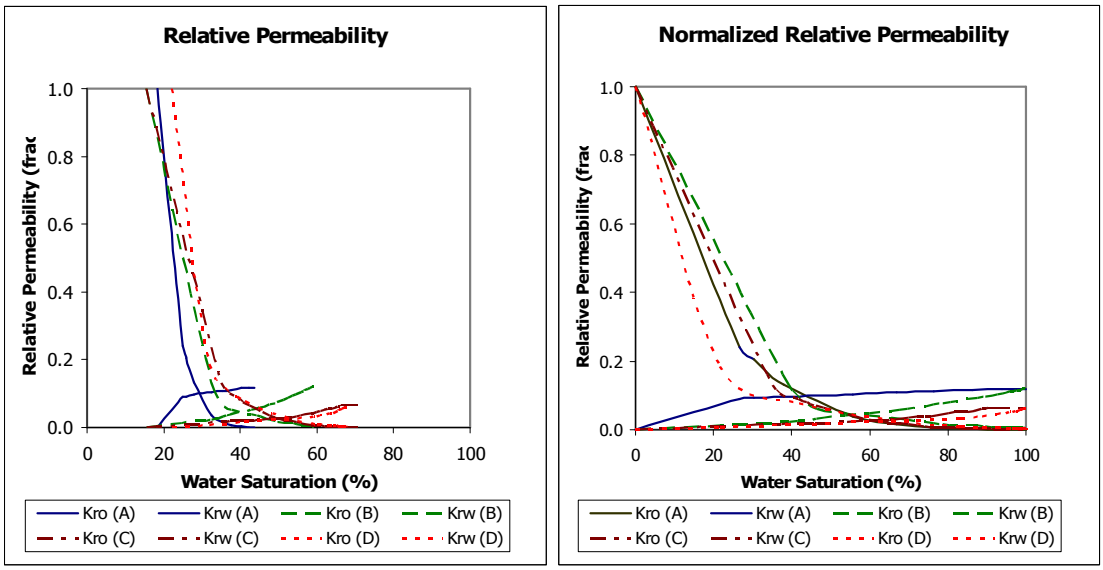

Figure 5.1 – Water-oil relative permeability curves as a function of water saturation.

The two phase oil-water at $S_g = 0$ and gas-oil relative permeability curves used for the CO_2 simulation are shown in Figures 5.2 and 5.3. To avoid complication and make the model simulation simple, this set of curves was used to describe both the oil column and the transition zone.

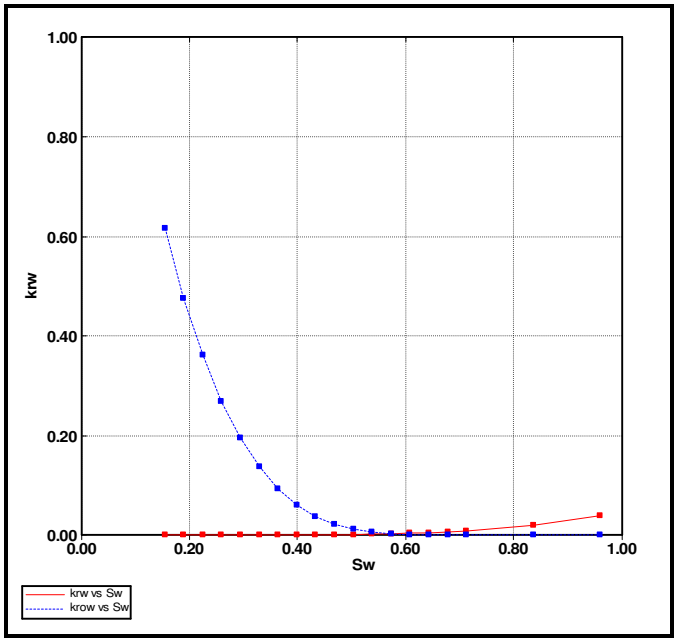

Figure 5.2 – Water-oil relative permeability curves.

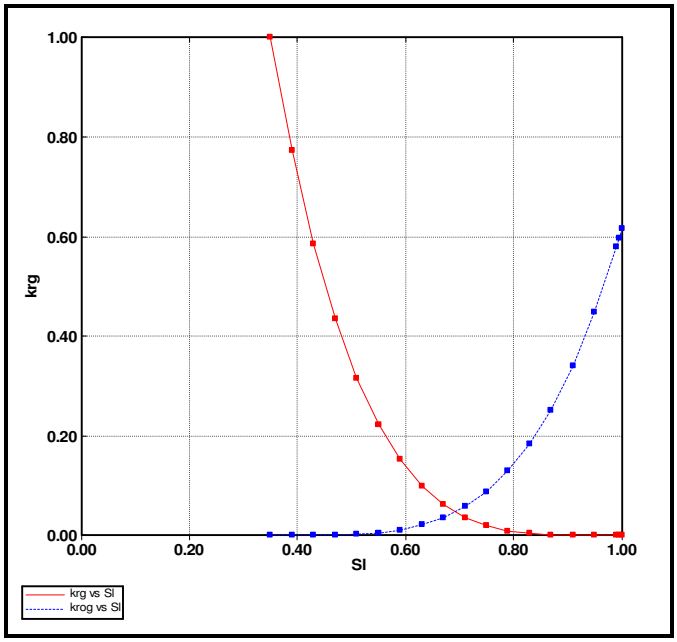

Figure 5.3 - Gas-oil relative permeability curves.

The maximum oil relative permeability is 0.65 at connate water saturation (S_{wc} = 15%). At 60% water saturation, the oil relative permeability is almost zero. As water saturation increases in the reservoir, the water relative permeability increases, reaching a maximum value of 0.04 at 94% water saturation.

Hysteresis effect is not considered in the simulation, after the drainage process of water displacing oil, CO_2 injection is going to be the governing displacement process.

5.2.2 Fracture Relative Permeability

A lot of research have been done in the characterization of relative permeability in fractures, it have been found that fracture aperture changes due to compaction,[22] mineralization and other factors affect the fluid flow. Roughness, capillary pressure and wettability constitute influence factors in the fluid flow interference; therefore, the assumption of straight lines in oil-water relative permeability would not the best representation.[23]

However, considering very high fracture permeability values, straight line relative permeability curves were used in this study.

5.3 Capillary Pressure

Three rock samples from Tensleep were selected for capillary pressure data, this samples were extracted from well 56-TPX-10; samples E (5391') and F (5400') and from well 44-1-TPX-10; sample G (5538').

The samples indicate a very similar lithological description, however, the initial water saturation values observed vary widely from 10.8% to 20.4%. Capillary pressure curves in the three samples show low displacement pressure (about 1 psi), this is an indication of good reservoir; very good sorting and big pore throats (W. Ahr, Carbonate Reservoir Course, Professor, Department of Geology and Geophysics, Texas A&M University).

Capillary pressure laboratory tests were performed using an air-brine system. These data were corrected to obtain oil-water capillary pressure values at reservoir conditions as shown in Figure 5.4. In order to do this correction, the following equation was applied:

$$Pc, res = \frac{(\sigma \cos\theta) res}{(\sigma \cos\theta) lab} Pc, lab$$

where σ is interfacial tension and θ is the contact angle.

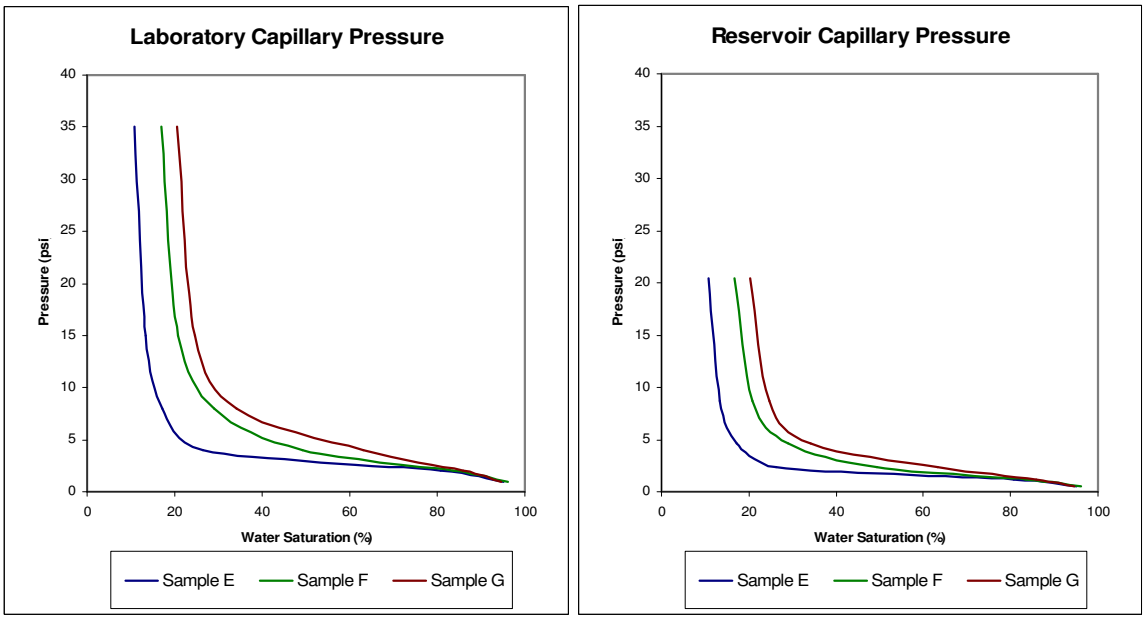

Figure 5.4- Capillary pressure curves at laboratory and reservoir conditions.

In order to account for porosity and permeability changes, normalization of capillary values, were conducted using the Leverett J function as follows:

$$J(S_n) = \frac{0.2166 * Pc}{(\sigma \cos\theta)} \sqrt{\frac{k}{\phi}}$$

Matrix capillary pressure was calculated from the average J curve using a regression of all data points in Sw vs. J plot as sown in Figure 5.5. Capillary pressure for fractures was assumed to be zero.

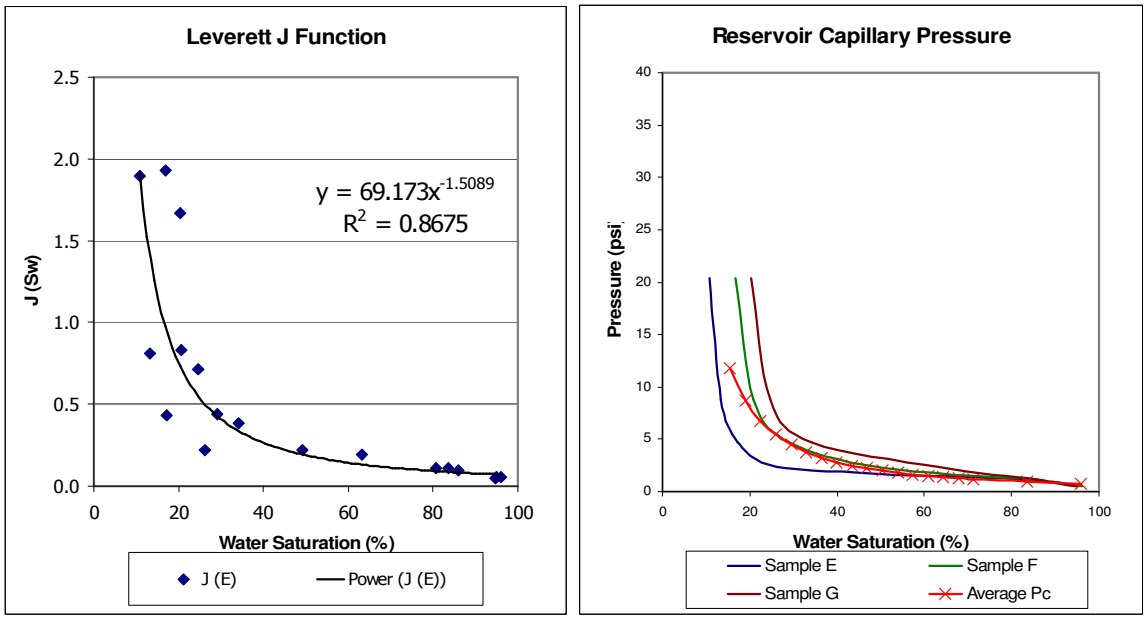

Figure 5.5 - Laboratory and average reservoir capillary pressure curves.

5.4 Wettability

A wettability test was performed in a core sample from the well 62-TPX-10 (5418') at reservoir temperature of 190 °F. Synthetic brine and crude oil were flushed through the sample. Evaluation of results provides a water-wet indicator of 0.402 versus oil-wet indicator of 0.033.

The water-wet indicator is a relation between the volume oil displaced spontaneously when the oil saturated rock sample is submerged in the synthetic brine, and the total oil volume displaced injecting brine in the sample up to residual oil saturation conditions.

5.5 Fracture Spacing

According with the measurements of fracture spacing in Tensleep core samples, a homogeneous matrix dimension of 10 ft were used in the dual-porosity simulation model.

5.6 Fluid Properties

The reservoir oil is sulfurous saturated black oil with a stock tank gravity of 31.4 °API and with a laboratory initial gas-oil ratio between 2 and 4 SCF/STB. Initial reservoir pressure and temperature are 2300 psi at reference depth of 5500 ft and 190 °F, bubble pressure and minimum miscibility pressure was determined experimentally to be of 42 psia and 1,300 psi respectively

5.6.1 PVT Information

Two bottom-hole oil samples were recollected and tested in the wells 54-TPX-10 (sample A) on June 15, 1984 and 62-TPX-10 (sample B) on April 28, 1986. The saturation pressure measured in the samples is between 61 to 76 psia. Very low value considering that higher saturation pressures can be expected in oil samples with stock tank API gravity of 31.4° and 31.1° in samples A and B, respectively. Table 5.1 shows the fluid composition.

Table 5.1 - Reservoir fluid composition in mole fractions.

Component	Mol Fraction		
	Sample A	Sample B	Sample C
CO_2	0.04	0.03	0.08
N_2	1.08	0.05	0.13
C_1	0.01	0.01	0.02
C_2	0.03	0.04	0.12
C_3	0.13	0.03	0.17
i-C_4	0.1	0.01	0.08
n-C_4	0.29	0.02	0.22
i-C_5	0.59	0.01	0.15
n-C_5	0.39	0.01	0.3
C_6	0.98	0.02	1.29
C_{7+}	96.36	99.7	97.44
Mw C_{7+}	285	270	303.85
Density $C_{7+ @ 60°F, gr/cm^3}$	0.8284	0.8694	0.8972
Temperature (°F)	190	190	190.4

Composition analysis for the samples A and B show very low content of light components, where almost 100% mole percent of plus fraction were found.

Fluid composition, constant composition expansion, differential liberation and separator tests were performed. Values of solution gas-oil ratio between 1 and 4 SCF/STB were measured at standard conditions and supported by the zero gas-oil ratio found in production reports. The amount of gas dissolved in the oil is very low and almost impossible to measure in the field.

A third PVT (sample C) was taken in 2004 from well 72-TPX-10 at surface conditions. Oil sample was recombined with a gas sample to obtain a reservoir fluid sample and performed a miscibility evaluation. Composition up to C_{30}+ was measured in this sample.

Constant composition expansion (CCE) was run on the reservoir fluid adding four (4) different CO_2 amounts for a known volume of reservoir fluid at reservoir temperature of 190.4 °F. Swelling Factor (SF), density and viscosity were measured for the different oil-CO_2 mixtures.

The three oil reservoir samples show the basic characteristics of the reservoir fluid have remained the same. Molar percentage of plus fraction between 95 to 98% and small oil-gas ratio were found. These data were used to tune an EOS capable of characterizing the CO_2/reservoir-oil system above the minimum miscibility pressure (MMP).

Table 5.2 lists the experiments and the measured parameters loaded into the PVT software.

Table 5.2 - PVT experimental data.

Experiment	Description
Reservoir Fluid Composition	Mole fractions, C_{30}+ density and molecular weight
Constant Composition Expansion	Relative Volumes, saturation pressure, oil density
Injection Test	Swelling test

Phase diagrams for samples A and C were generated to evaluate the possible changes of the reservoir fluid characteristics after two decades of production. The two phase diagrams are representatives of black oil fluids. At reservoir temperature phase diagrams show a saturation pressure near 20 psi, this value is lower than the values measured in the lab from the two samples.

Sample C, the latest oil sample was chosen to evaluate the reservoir simulation of CO_2 injection process, because it is the only tests that includes swelling information.

5.7 Fluid Model Selection

In compositional simulation, the computational time is proportional to the number of components considered in the fluids model. Therefore it is necessary to evaluate the effect of the number of components in the EOS tuning, this considering that the sample with swelling information is characterized up to C_{30}+ component.

Two different compositions were used, the original components that goes up to C_{30}+ and a compressed one with components up to C_6+. For the last one, plus component was splitted into five pseudo-components. Simulation results from the compressed components were compared with the results from the original components. The results of these simulations are presented late in this chapter. The fluid models have different critical points and the phase diagrams. However at reservoir temperature (190 °F) the equilibrium lines of initial component behave very similar to those for the compressed components as shown in Figure 5.6.

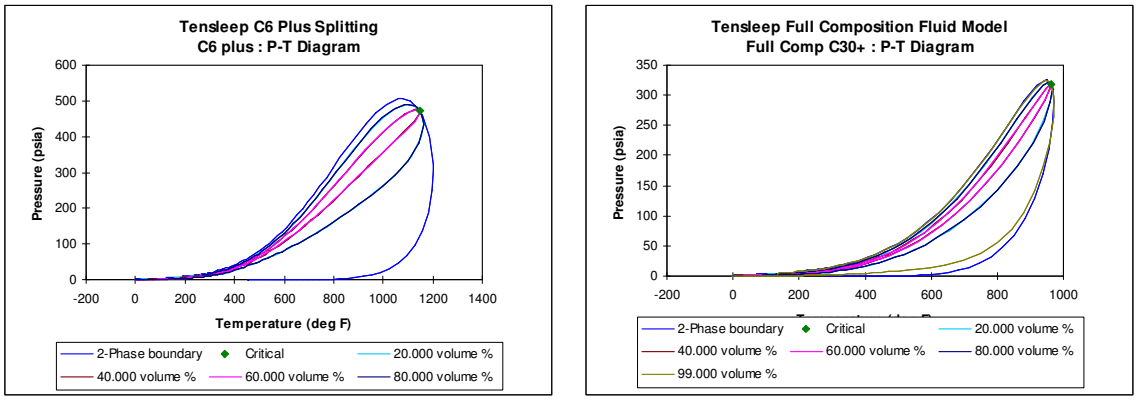

Figure 5.6- Phase diagrams for C_6+ and C_{30}+.

5.7.1 Equation-of-State Characterization

CO_2 injection in an oil reservoir as a miscible process needs the best phase equilibrium prediction during the CO_2 injection process. EOS has general acceptance as tools calculate the complex phase behavior associated with rich condensates, volatile oils and gas injection processes.[24] Tuning an equation-of-state (EOS) that reproduces the observed fluid behavior is required to accurately predict the CO_2 /oil phase behavior in the compositional simulation.

WinProp, a CMG™ software was used in the EOS tuning process. The characterization of CO2-oil mixtures process follows the methodology suggested by Khan.[25] The Peng-Robinson[26] EOS was chosen because it is applicable for low-temperature CO_2/oil mixtures.[25] The viscosity model from Lohrenz-Bray-Clark (LBC)[27] was considered.

5.7.2 EOS Tuning Process for C_6+ Sample

PVT simulation model for EOS tuning process was performed using Peng-Robinson EOS. First, a model with no regression of any parameters (Initial curve) was run. Then a second model by changing plus fraction critical properties and binary interaction coefficients between CO_2 and the plus fraction (Final curve) was generated, (Figure 5.7).

Results from the runs show a very poor reproduction of the laboratory observations (PVT-lab). Neither the original Peng-Robinson EOS nor the modified EOS with regressed C_6+ critical properties could reproduce swelling factor and saturation pressure.

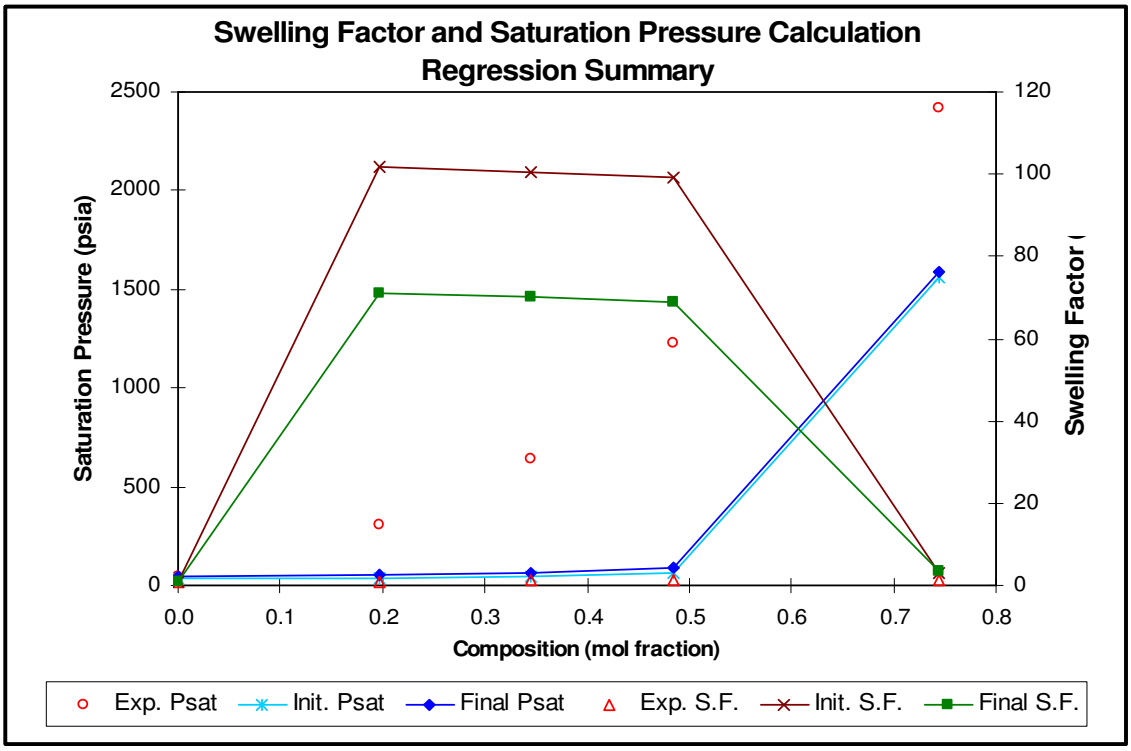

Figure 5.7 - Initial swelling factor for C_6+ sample.

The EOS tuning was a multi-step process starting by splitting the heavy component C6+ as proposed by Whitson.[28] Whitson's method uses a three-parameter gamma probability function to characterize the molar distribution (mole fraction / molecular weight relation) and physical properties of petroleum fractions such as heptanes-plus (C_7 +), preserving the molecular weight of the plus fraction.[29] This method is used to enhance the EOS predictions.

Since a single heavy fraction lumps thousands of compounds with a carbon number higher than seven, the properties of the heavy component C_7+ are usually not known precisely, and thus represent the main source of error in the EOS and reducing its predictive accuracy. For this reason, regressions were performed against the pseudo-components to improve the EOS predictions.

The C_6+ component was splitted into five pseudo-components based on its relative mole fraction as suggested by Khan.[25] The pseudo components were identified as C_6-C_{12}(1), C_{13}-C_{19}(2), C_{20}-C_{27}(3), C_{28}-C_{29}(4) and C_{30}+. By splitting the heavy component (C_6+), the total number of components of the reservoir fluid was then increased from 9 to 13 components. This 13-component mixture was used to tune the EOS to match data.

WinProp™ suggest some parameters to be changed in an initial regression. A total of 21 parameters were changed including critical pressure (Pc), critical temperature (Tc), critical volume (Vc), molecular weight (MW) of the heavy pseudo-components. Also binary interaction coefficients between the carbon dioxide and the heavy pseudo-components were modified. Although a good match was achieved, this model is not efficient, because many number of parameters need to be modified to match laboratory data.

In the attempt to reduce the number of parameters to be changed and preserve the EOS as original as possible, several models with less number of parameters were run.

Finally, only modifications of the heaviest pseudo component C_{30}+ critical properties (Pc and Tc), and binary interaction coefficients CO_2-C_1 and CO_2-C_{30}+ were necessary to match swelling data (Figure 5.8). Swelling factor is not only function of the amount of CO_2 dissolved, but also of the size of the oil molecules.[30] Plus fraction molar weight was also used as regression parameter to obtain a confident match in the swelling and saturation pressure calculation.

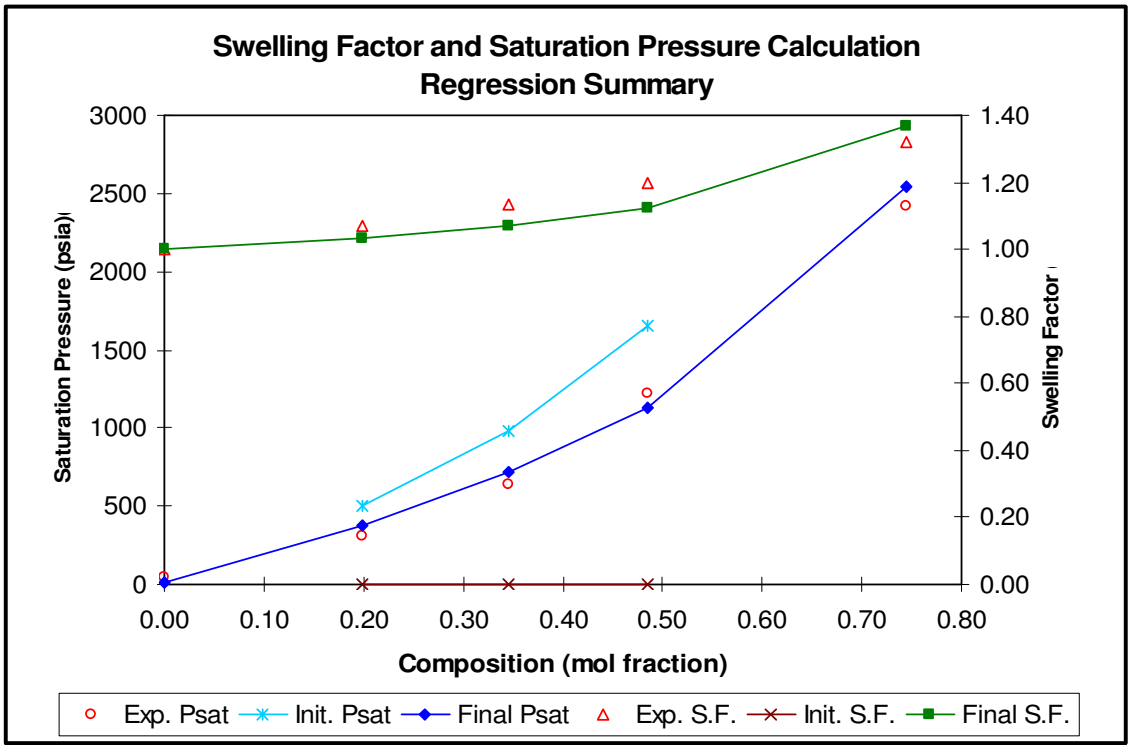

Figure 5.8 - Match of swelling factor splitting C_6+.

Simultaneously the sample with composition up to C_{30}+ was tuned following the same procedure described before. No splitting process was applied to the C_{30}+ component. The regression parameters used to match the swelling experiment were Pc, Tc and molecular weight in the heaviest pseudo-component, as in the C_6+ sample.

A reservoir fluid model with 30 components represents a large number of equations to be solved in reservoir simulation, which is the reason why this model is not practical in terms of simulation running time.

Pseudoize, group or lump the components into a fewer number of pseudo-components is performed primarily for speeding up the simulation running time. Fewer components result in faster run time. The Fevang[31] lumping process consists of forming new pseudo-components from existing 13 was used.

Similar component properties and molecular weight were the criteria for lumping the pseudo-components. Several numbers of regressions were necessary to select the best grouping scheme for tuning laboratory experiments.

Finally a 9-component EOS fluid model was obtained after grouping $C_2 + C_3$, $iC_4 + nC_4 + iC_5 + nC_5$, leaving the remaining components ungrouped.

New regression of EOS parameters is necessary. As in the no-lumped fluid model, only critical properties of the heaviest fraction ($C_{30}+$) and the interaction coefficient parameters between CO_2-C_1 and CO_2-$C_{30}+$ were necessary to match laboratory data. After performing these regressions, the PVT properties of the 9-component EOS model matched closely with the 13-component EOS model, (Figure 5.9).

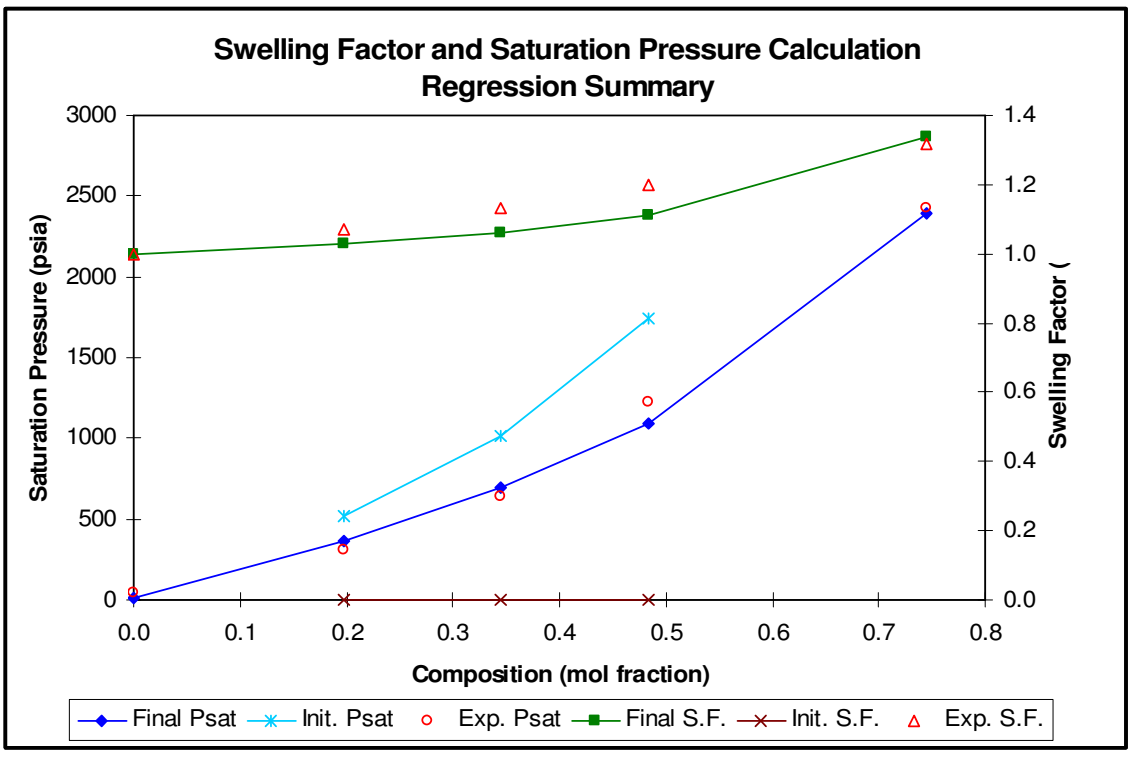

Figure 5.9 - Match of swelling factor using lumped model.

The low saturation pressure of the reservoir fluid measured in the laboratory (42 psia) indicates that the oil is currently in under-saturation conditions. No oil viscosity or density under saturation pressure was measured in the laboratory.

The low gas oil ratio (4 SCF/STB) measured in the field, suggests that no big variations in reservoir fluid viscosity or density can be expected when CO_2 is injected. In the mean time viscosity and oil density measured above saturation pressure at different CO_2 mole fractions could not be represented by PR-EOS.

5.7.3 Tuned Fluid Sample Evaluation

Lumped and no lumped fluid samples reproduce the experimental swelling factor very well, however several lump schemes could match laboratory data while provide different results when they are used in reservoir simulation.

Taking into consideration that only swelling factor test is available for Tensleep oil to tune the EOS, evaluation of the two fluid samples (lumped and no lumped) using a synthetic reservoir model was performed.

A quarter of a 40-acre inverted five spot pattern was built. The 10 acres single porosity model contains two vertical wells, one producer and one injector. The 20 x 20 x 1 grid contains 4000 cells with 66 ft on the sides. Rock properties were taken from core analysis and compositional fluid model for C_6+ was used in the comparison.

Porosity and permeability modifications were applied to the peripheral cells to avoid adding extra pore volume to the one quarter of pattern. Well fraction in producer and injector were set to 0.25.

Two compositional fluid models, one from the lumped sample and one from the no lumped sample were used in a simulation model. Different oil production behaviors were observed for those two models.

Lumped simulation model can not maintain oil production for the same period as the no-lumped model. Drop in oil rate is related with gas breakthrough, this occurs six months earlier than in no-lumped fluid model as shown in Figure 5.10. This unexpected result, suggests that further reservoir fluid characterization is required.

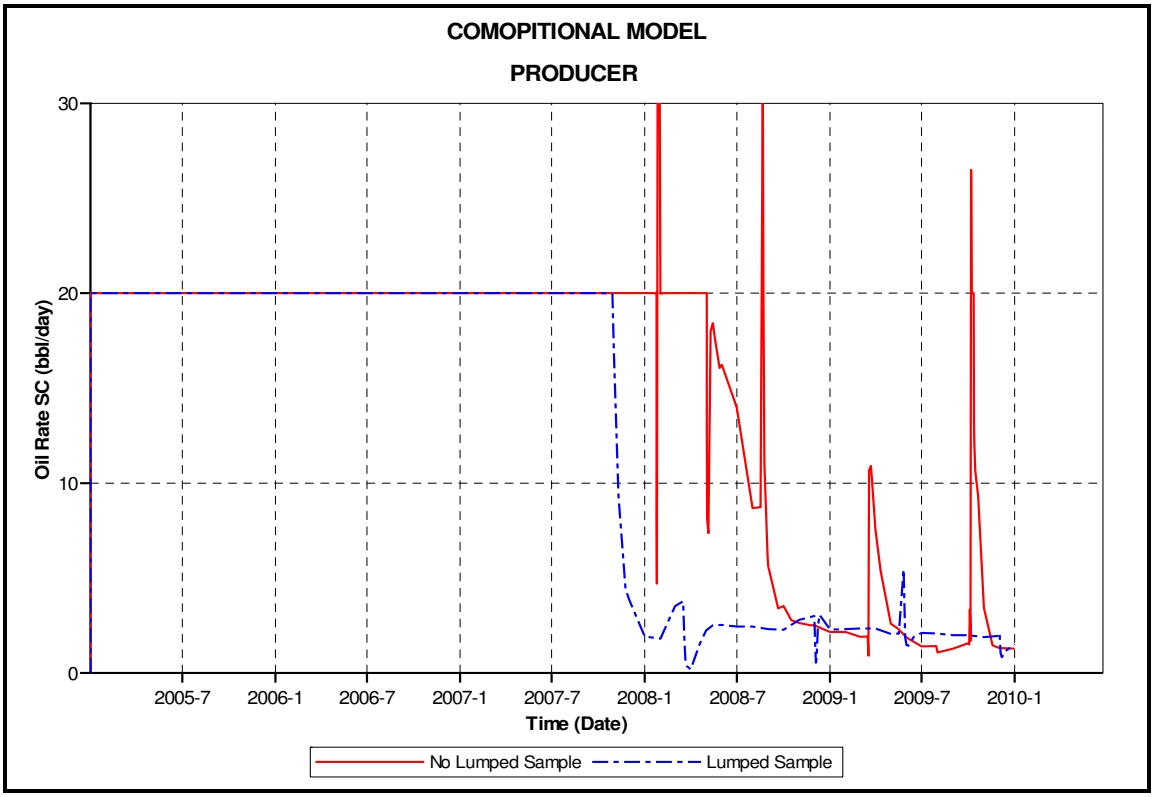

Figure 5.10 – Comparison of oil production between lumped and no lumped fluid model.

No-lumped sample can be considered as the original fluid sample, this fluid model represent the behavior of reservoir fluid under CO_2 injection process.

To understand how the number of components in the fluid sample or the reservoir fluid model can affect reservoir simulation performance, evaluation of different fluid samples will be carry on as follows.

Table 5.3 summarizes the best fit parameters of Peng-Robinson EOS obtained for the splitted, no-lumped C6+ sample

Table 5.3 - Description of Tensleep reservoir fluid sample.

Component	Mw	Pc (atm)	Tc (K)	Omega A	Omega B	Acentric Factor	Vc (ft3/lb-mol)	Zc
CO_2	44.0	72.8	304.2	0.4572	0.0778	0.225	0.094	0.274
C_1	16.0	45.4	190.6	0.4572	0.0778	0.008	0.099	0.288
C_2	30.1	48.2	305.4	0.4572	0.0778	0.098	0.148	0.279
C_3	44.1	41.9	369.8	0.4572	0.0778	0.152	0.203	0.276
iC_4	58.1	36.0	408.1	0.4572	0.0778	0.176	0.263	0.275
nC_4	58.1	37.5	425.2	0.4572	0.0778	0.193	0.255	0.273
iC_5	72.2	33.4	460.4	0.4572	0.0778	0.227	0.306	0.272
nC_5	72.2	33.3	469.6	0.4572	0.0778	0.251	0.304	0.269
C_6-C_{12}	121.2	26.9	592.5	0.4572	0.0778	0.342	0.468	0.265
C_{13}-C_{19}	219.4	17.6	732.5	0.4572	0.0778	0.595	0.809	0.253
C_{20}-C_{27}	323.5	13.4	829.0	0.4572	0.0778	0.823	1.114	0.248
C_{28}-C_{29}	398.0	11.5	884.3	0.4572	0.0778	0.981	1.307	0.244
C_{30}+	637.6	8.1	1030.0	0.4572	0.0778	1.289	1.816	0.234

5.8 Compositional vs. Pseudo-Miscible Models

Compositional simulation is commonly used in CO_2 flooding process. This model predicts the multi-contact miscibility gas-oil process as the surface tension between the two hydrocarbon phases drops to zero.

Pseudo-miscible model only defines the amount of injected gas that is miscible with the hydrocarbons in the reservoir. Pseudo-miscible model is based on the empirical treatment suggested by M. Todd and W. Longstaff[21] to represent miscible processes without going into the complexity of compositional models.

Pseudo-miscible model considers three components system, reservoir oil, injection gas (solvent) and water. The reservoir oil component consists of stock tank oil together with the associated solution gas. The solvent and reservoir oil components are assumed to be miscible in all proportions and consequently only one hydrocarbon phase exists in the reservoir.

Tensleep reservoir fluid can be considered as dead oil. Small interaction between CO_2 and the scare light components in the oil is expected.

In this study, I evaluate the use of pseudo-miscible fluid models to describe the CO_2 injection process in Tensleep Formation. Results from this model were compared with results from compositional simulation. Pseudo-miscible model was considered because is faster as previous discussed.

Results provided from the pseudo-miscible and compositional models show that for Tensleep reservoir fluid, pseudo-miscible option do not behave closely to the compositional approach.

Tuned PR-EOS was used to generate two oil PVT models (C_6+ and C_{30}+) for pseudo-miscible and compositional simulators. The synthetic reservoir model mentioned before was used.

5.8.1 Comparison of Pseudo-Miscible C_6+ and C_{30}+ Models

Two pseudo-miscible simulation models were generated. One of the models used fluid description with components up to C_6+ and other using components up to C_{30}+. Oil and gas production rates and reservoir pressure were plotted to describe the effect of the number of components on oil production rate.

Both fluid samples show similar oil rate production profile, CO_2 breakthrough time differs on one month, 6% of the time, (Figure 5.11). Only slight differences in the

average reservoir pressure are observed; reservoir pressure drops slightly faster in the C_{30}+ model.

These results suggest that to save simulation running time, C_6+ fluid sample can be used in the field simulation model with assurance.

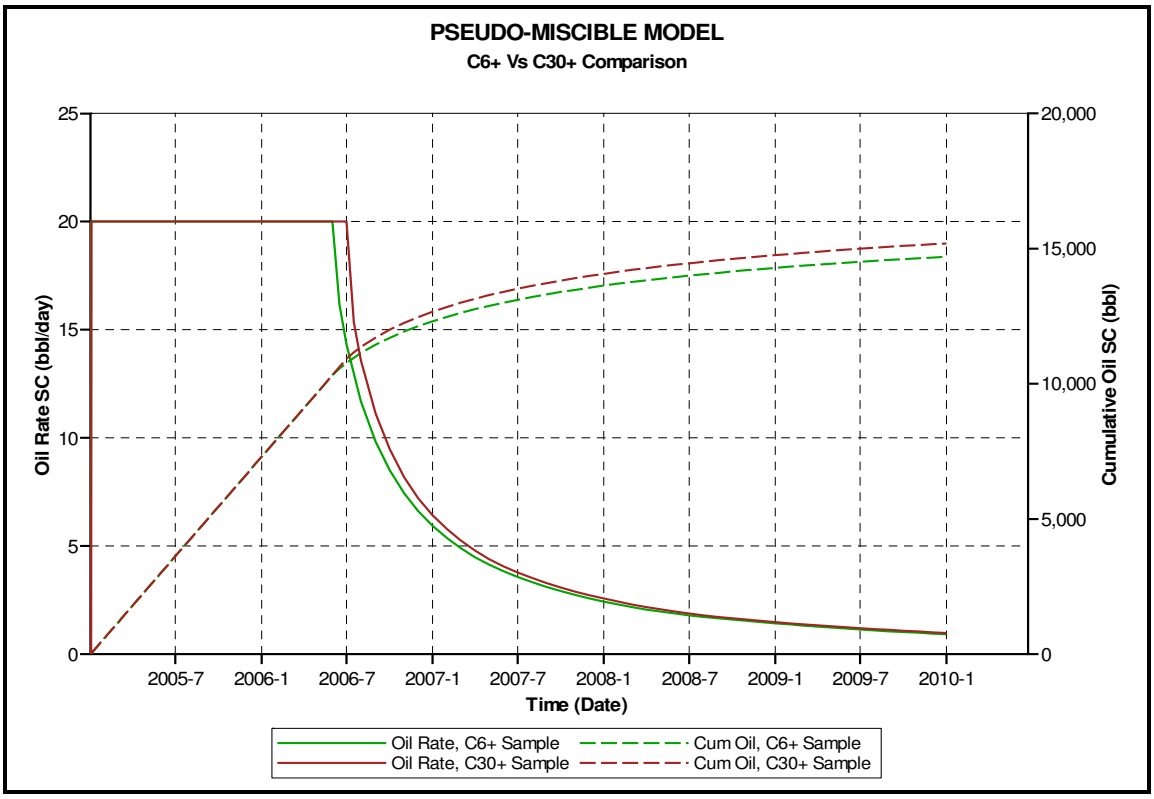

Figure 5.11 - Qo and Np for pseudo-miscible models C_6+ vs C_{30}+.

5.8.2 Comparison of Compositional C_6+ and C_{30}+ Models

Using the compositional fluid models, similar behavior as in the pseudo-miscible model was observed. Similar CO_2 breakthrough time was obtained from the two fluid models. Flat oil production period last for 3.5 years, this is two more years than in pseudo-miscible model, (Figure 5.12).

As the objective of the CO_2 storage is to maximize the amount of gas dissolved in the reservoir fluid, a late gas breakthrough time is desired. After gas breakthrough occurs, commonly liquid production is constrained to avoid gas recirculation.

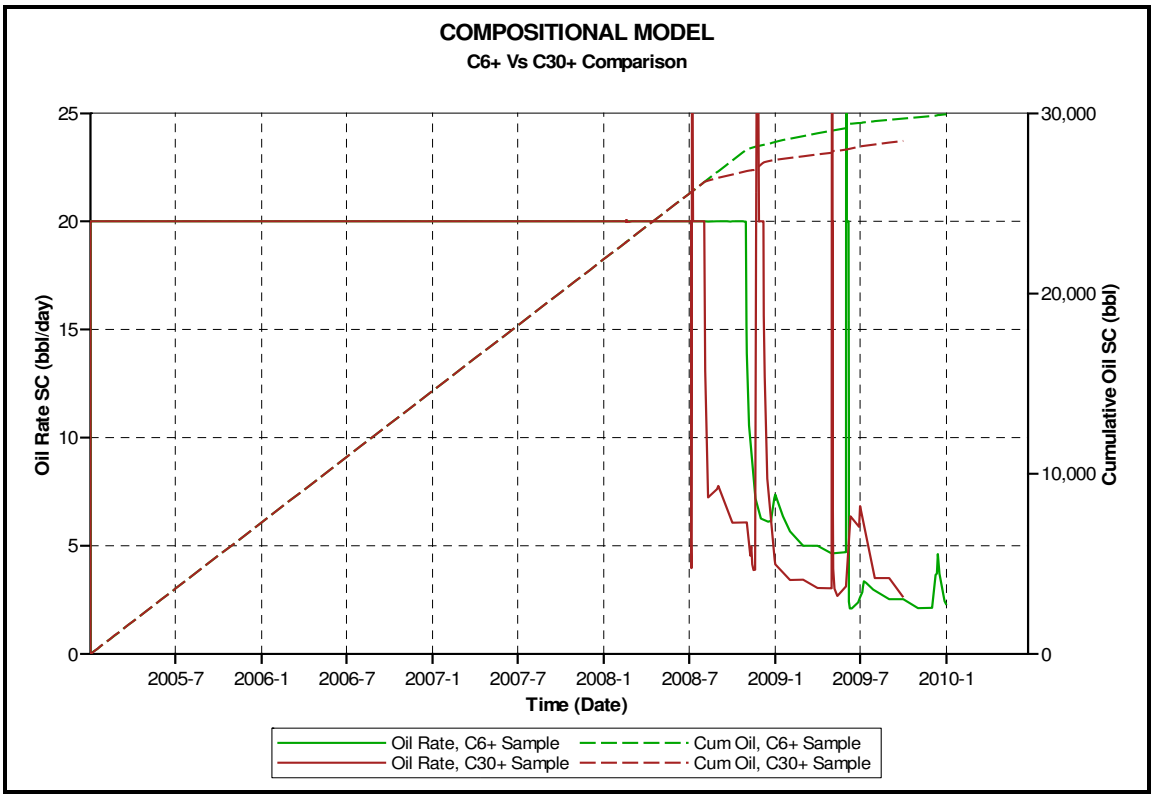

Figure 5.12- Qo and Np for compositional models C_6+ vs C_{30}+.

Comparison of compositional fluid models provides similar results as in pseudo-miscible models. However in this case using C_6+ sample a difference of 4 months in gas breakthrough time are observed, this is a 7% more time than using C_{30}+ model.

Compositional simulation also demonstrates that C_6+ fluid model can be used with confidence, this reducing simulation complexity and run time.

5.8.3 Comparison of Compositional and Pseudo-Miscible Models

From previous fluid evaluation have been recognized that no-lumped C_6+ fluid sample can be used in the numerical simulation of CO_2 storage in Tensleep Formation. Now it is necessary to establish which fluid model, pseudo-miscible or compositional should be used in order to have accurate forecast results.

Figure 5.13 shows oil production performance from the two models. Earlier gas breakthrough is observed in the pseudo-miscible model, then lower cumulative oil production is obtained. Basically, compositional fluid model produces twice the oil volume than pseudo-miscible model.

This is a big difference, considering that due to the dead oil characteristic of Tensleep reservoir fluid; similar oil production behavior can be expected from the two fluid models.

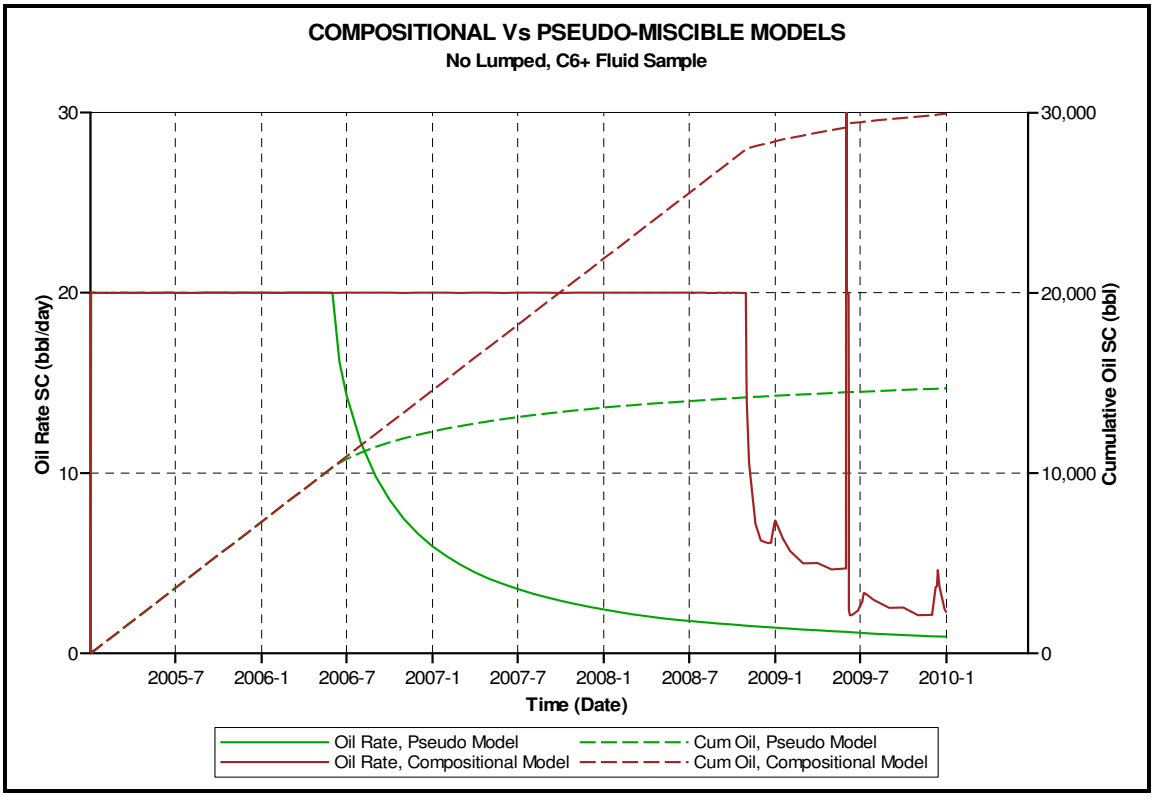

Figure 5.13 - Qo and Np for compositional and pseudo-miscible models.

In pseudo-miscible reservoir simulation model 70% of the CO_2 injected is miscible with the dead oil. Not dissolved gas acts like a piston displacing the oil and accelerating the gas breakthrough.

Commonly CO_2 injection process is represented with compositional simulation.

Results from compositional and pseudo-miscible numerical simulation models provides evidence that to represent a CO_2 storage process in Tensleep Formation it is necessary to use the compositional approach.

5.9 Reservoir Simulation Model

The reservoir simulation model covers 400 acres and contains 15 production wells. All the wells are vertical and completed in the 4th layer of the simulation model. The grid was 50 x 30 x 6 with 9000 total cells in the model. There are 5088 active cells with 300 x 300 ft. The model consists of the main faults that limit the structure at west and north locations. Figure 5.14 shows a 3D view of the simulation grid for Teapot Dome field.

Six layers described in the geologic model of Tensleep Formation as main units, represent an intercalation of sandstones and dolomites. Layers 1, 3 and 5 were defined as dolomites with low matrix porosity and low permeability. Layers 2, 4 and 6 are sandstones with better values of porosity and permeability. The main productive unit is located in 4th layer.

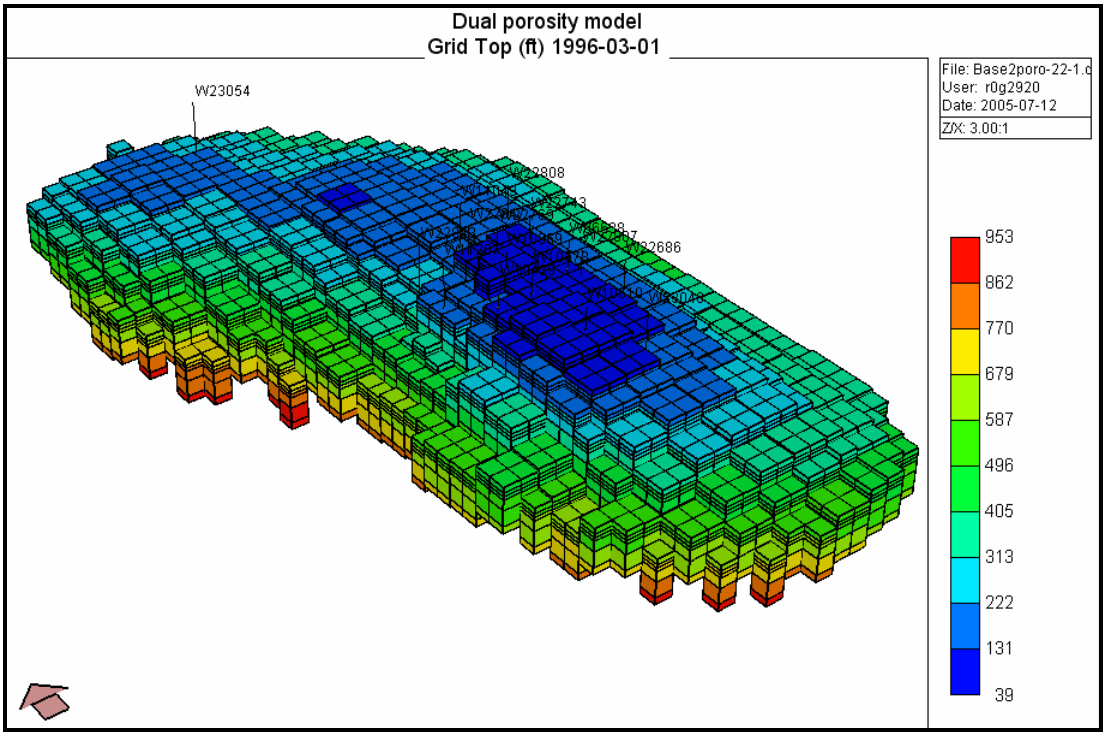

Figure 5.14 - Simulation grid for Tensleep Formation.

All the layers have a constant thickness as determined from the subdivision in the log type. Porosity for each layer is an average value calculated from porosity values measured in cores.

Air permeabilities values were assumed as total permeability for layers 2, 4 and 6. Vertical permeability was obtained from k_h/k_v correlations derived from core measurements taken from Well 48-X-28. Table 5.4 lists the values of permeability, porosity and net pay of each layer in the simulation model.

Table 5.4 - Net pay, porosity and permeability in the simulation model.

Layer	Thickness (ft)	Net Pay (fraction)	Porosity (%)	Horizontal K (mD)	Vertical K (mD
1	30	0.1	1.0	1	0.1
2	20	0.1	13.5	50	9.5
3	20	0.1	1.0	1	0.1
4	60	0.1	13.5	50	9.5
5	90	0.1	1.0	1	0.1
6	40	0.1	13.5	50	9.5

5.9.1 Initial Conditions

Reservoir simulation model was initiated at a uniform pressure of 2300 psia @ 200 ft sub sea and constant temperature of 190°F. The initial water saturation from the relative permeability curve was 0.15. Initial oil saturation within the grid blocks was 0.85.

The simulation model contains an estimate of 4.5 million barrels of OOIP at the initialization stage.

5.9.2 Aquifer Representation

An analytical aquifer was selected to represent the strong water influx in the reservoir. This is a modified Van-Everdingen and Hurst method. It changes the assumption from

"a field producing at a constant hydrocarbon rate" to "an aquifer with influx water at a constant rate". This assumption simplifies the solution implemented in the simulator.[19]

The precise extension and strength is not known because no pressure data have been collected from the reservoir.

CHAPTER VI

HISTORY MATCHING

In this chapter the technique to reproduce historical fluid production rates and field pressure behavior is presented, along with validating and tuning the geological model to predict the future performance of the reservoir in different scenarios.

Initially, Black oil simulator IMEX^{TM} was used as a first approximation to evaluate the accuracy of the simulation models. Black oil simulator is simplest in terms of reservoir fluid description; this is the reason why it runs faster than compositional simulation.

As described in the geological evaluation, Teapot Dome formation is a highly fractured formation. Effects of fractures in reservoir fluids production will be evaluated. Single porosity simulation model results will be compared with those from dual porosity model.

Dual porosity models with constant and variable fracture permeability will be compared. Variable fracture permeability will be generated fracture aperture using the cubic law. Has been found that fracture aperture measured with X-Ray CT scanner follows lognormal distribution.

Historical oil production and water rates of each well were used with the simulation results to compare the effectiveness of those models. Gas production was not considered due to the dead oil nature of the reservoir fluid. The quality of the models was judged from how well the simulated water and oil production rates fit with historical data.

Analytical aquifer was used to reproduce the slight pressure drop present in the field. Size and strength of the aquifer were defined by trial and error process.

The matching of historical performance was performed to test the validity of the simulation model and to prepare the model for the prediction of the future reservoir performance.

Summary of the simulation models used in the history match and its main characteristics are described in Table 6.1.

Table 6.1. Reservoir simulation cases.

Case	Porosity Model	Fracture K (mD)	Cummulative Water (MM STB)	% Difference
CASE-1	Single	N.A.	3	98%
CASE-2	Single	N.A.	9	94%
CASE-3	Dual	1,000	16	89%
CASE-4	Dual	10,000	83	45%
CASE-5	Dual	100,000	84	44%
CASE-6	Dual	10000-20000	116	23%
CASE-7	Dual	10000-60000	135	10%
CASE-8	Dual Porosity Model, Compositional Fluid Model			
CASE-9	Dual Porosity Model, Pseudo-miscible Model			

6.1 Aquifer Dimensioning

A trial and error approach was used to establish the proper aquifer size and strength. Using an analytical Carter-Tracy aquifer connected at the bottom of the simulation grid, with 1500 ft thickness, 8% porosity, 1000 mD permeability of and 30000 ft radius size the assumed pressure drop could be reproduced. The model could approximately reproduce reservoir pressure as well as water production rates, (Figure 6.1).

6.2 Single Porosity Model

Single porosity model is commonly used in the reservoir simulation of detritus formations where intergranular porosity is considered the main storage and fluid flow media. In this case permeability is function of pore throat size, pore space tortuosity, shale content and mineralization through the rock pores.

In the CASE-1, relative permeabilities and capillary pressure measured in the cores were used. As expected, this model is limited to reproduce the high water production volumes observed in the field. Although the model can reproduce specified oil rates, water breakthrough times are too long and water rates are less than the observed values.

In an attempt to increase the field water production, capillary pressure, OWC depth and vertical permeability were changed. However the field water production can not match the observed data.

In the simulation CASE-2 a straight line for water relative permeability from 0 ($S_w = S_{wc}$) to 0.5 ($S_w = 1-S_{or}$) was used to increase water mobility. Even though, this change increase water rate but it is still not enough to reach historical water production rates, (Figure 6.1).

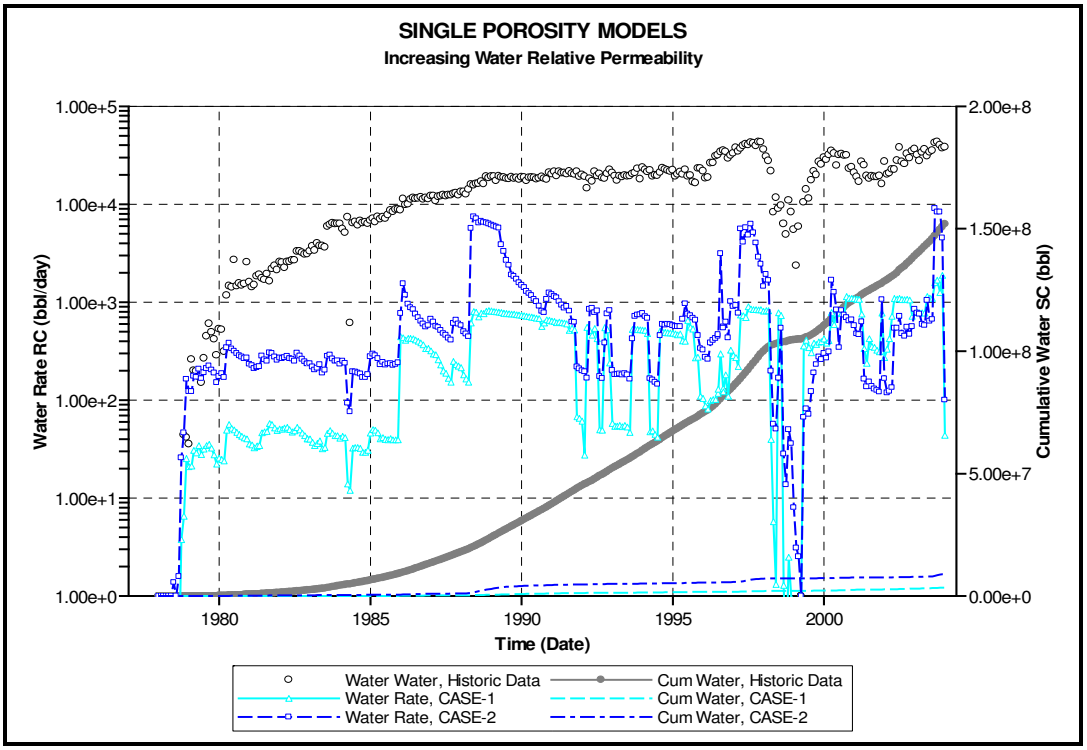

Figure 6.1 - Water production in single porosity models.

A reservoir model that has high permeability channels is required. Fractures will improve water flow thorough the reservoir, then field water production can be reproduced.

6.3 Dual Porosity Model

Dual porosity model, consider that fluids exist in two interconnected systems; the rock matrix, which usually provides the bulk of the reservoir volume and fractures which provide the main flow path. Traditional approach uses a constant fracture permeability value. This study uses variable fracture permeability calculated from fracture aperture distribution measured in fracture core samples.

6.3.1 Constant Fracture Permeability

In order to investigate the effect of fractures in reservoir performances, a constant fracture permeability of 1000 mD was used as an initial approach (CASE-3). This model was compared to single porosity model. Figure 6.2 shows the potential of using the dual porosity model to reproduce field production. Introduced fractures in the reservoir model improve simulated water rates. The fracture permeability is one of main issues in using dual porosity model. Usually permeability values obtained from pressure build-up test analysis are used. Permeabilities are tuned to match production rates and bottom-hole pressures in the tested well. Unfortunately in Teapot Dome, field pressure information in the Tensleep Formation is not available and a comparison with wells data is not possible.

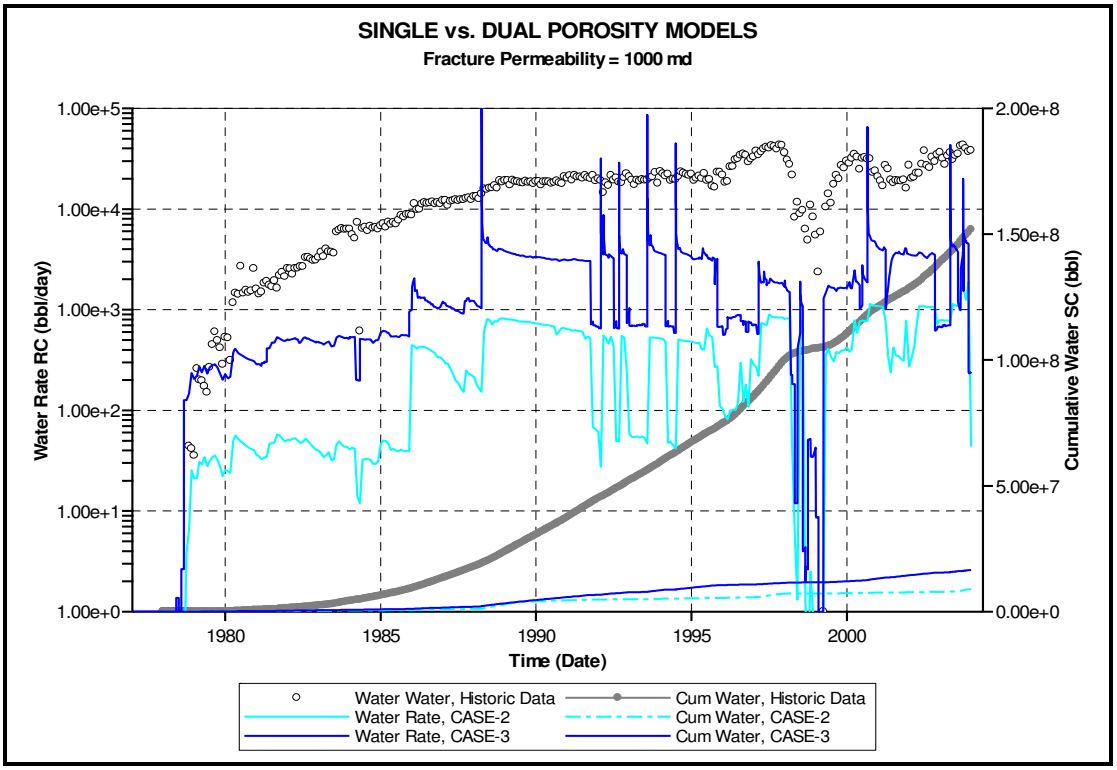

Figure 6.2 - Water production, dual and single porosity models.

Three cases with different fracture permeability values were run to investigate the magnitude of fracture permeability values that could reproduce observed water production. The cases are defined as CASE-3 with a permeability of 1.000 mD, CASE-4 with 10.000 mD and CASE-5 with 100.000 mD.

The CASE-4 results show a significant improvement compared to CASE-3, (Figure 6.3). The CASE-4 model could give a closer water production to observed data.

In the mean time, CASE-5 that has higher fracture permeability produces extremely high water rate at initial period. After 20 years of field production cumulative water produced is one third the historic value, At this time the average reservoir pressure have dropped more than 1500 psi and the model is not able to produce the oil rate constrained.

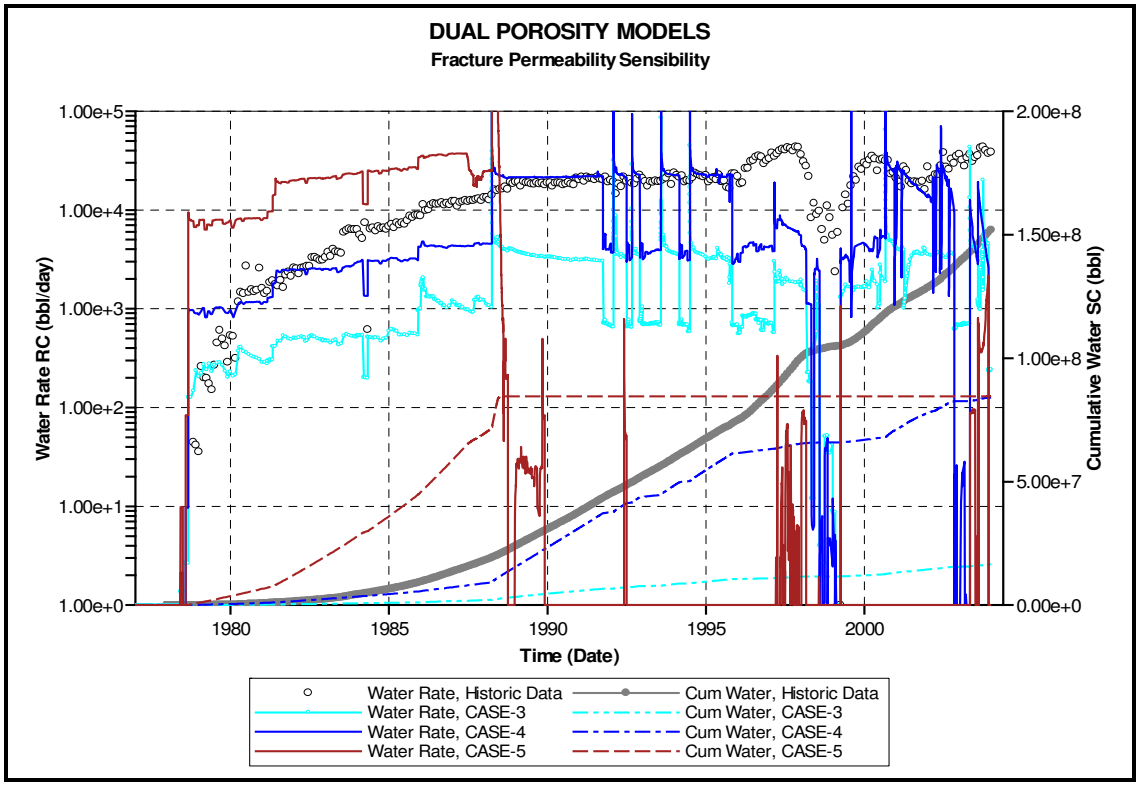

Figure 6.3 - Water production of dual porosity models with constant Kf.

Even though the CASE-4 shows a promising result but the use of constant fracture permeability is difficult to accept. As all we know fracture surfaces are rough due to the natural rock braking process and for the presence of certain minerals formed by mineralization or cementation, therefore the permeability fracture is not constant, (Figure 6.4).

Figure 6.4 – Natural fracture face.

6.2.2 Variable Fracture Permeability

In this study we utilized a 4th generation X-Ray CT computerized tomography (CT) scanner to measure fracture aperture from Tensleep Formation core sample. The X-Ray CT scanner is one of the non-intrusive techniques widely used to determine rock properties and visualize fluid flow through porous media. Several CT applications[9, 10, 11, 12, 13, 14] include study of heterogeneous rocks, fractures, vuggy carbonates and determination of porosity and bulk density. The CT images have been used to analyze

oil bypassing, CO_2 injection reduction using surfactants and water alternate gas process, to name a few.

A core sample of 2.5 in. with a natural mineralized fracture from Tensleep Formation was used to measure fracture aperture distribution (Figure 6.5).

The results of CT scan images are shown in Figure 6.6. CT images clearly show that fracture penetrates the core sample. This fracture aperture was measured with our previous techniques.[19]

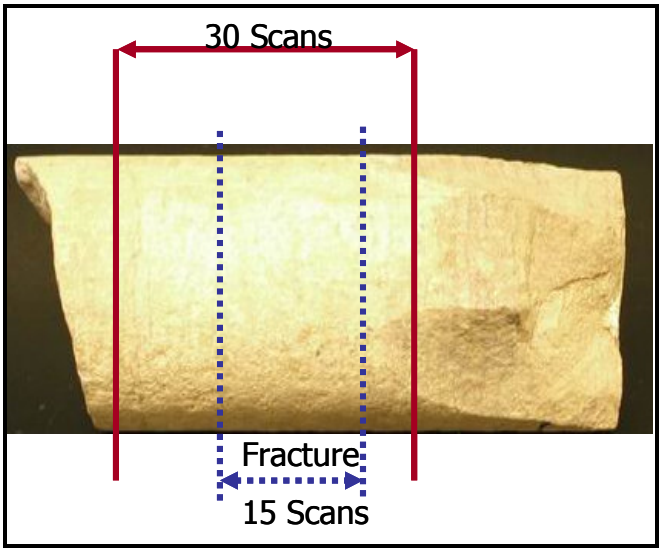

Figure 6.5 - Tensleep fractured core sample.

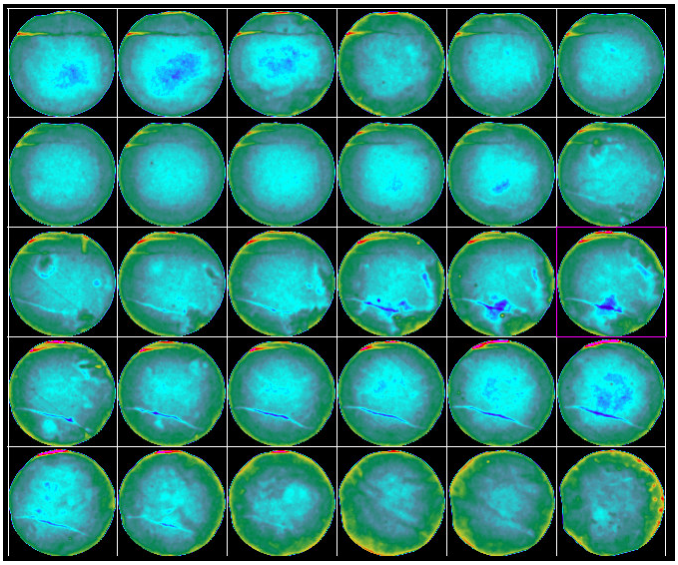

Figure 6.6 – CT X-Ray images from Tensleep core sample.

The X-Ray CT scan measure CT Number, this is function of the material density. As density do not represent fracture aperture, a calibration process to calculate aperture from CT Number is then needed. A rock specimen from unfractured part of a Tensleep core is cut using a diamond saw along the longitudinal direction. Cut faces were grinded using a grinding machine to reduce surface roughness as much as possible. Feeler gauges of 51 μm, 76 μm, 203 μm, 279 μm, 330 μm were inserted between the halves to obtain small fracture known apertures.

Multiple CT scans were taken in the middle of the core between the two feeler gauges. The more dense area is shown with an orange color and less dense area is shown green, blue and black in decreasing order of density.

Although the matrix and the fracture can be clearly distinguished with CT number, it is impossible to determine the aperture size with CT number only. However, this CT numbers correspond to a known fracture size in μm, (Figure 6.7).

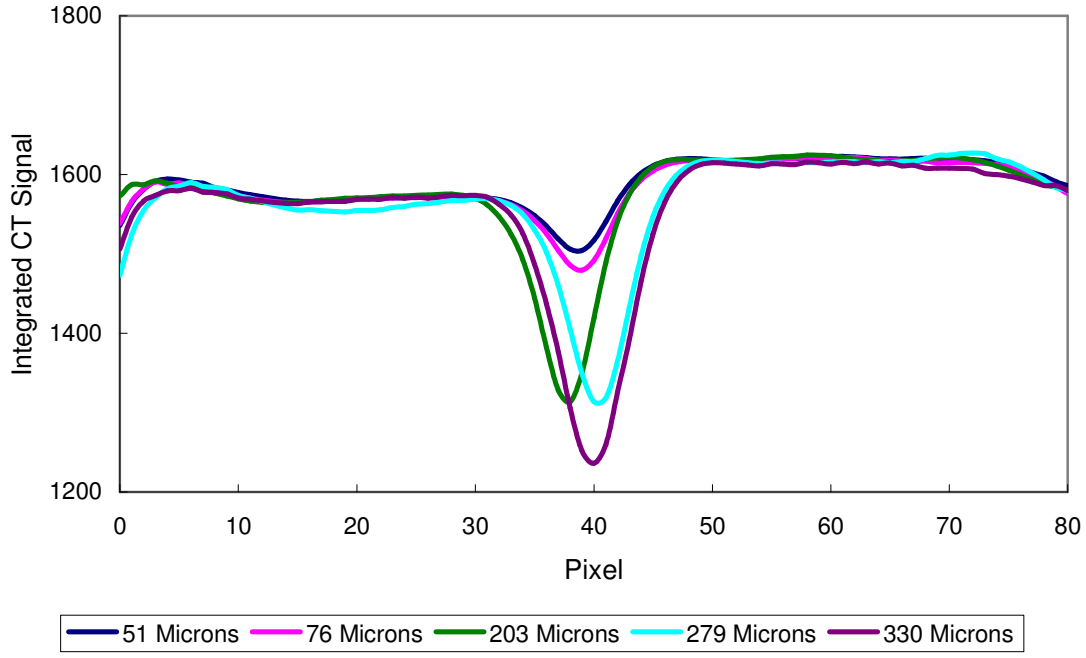

Figure 6.7 – Comparison of CT number plots for different fracture sizes.

We found that if the feeler gauge size increases the CT numbers of fracture decrease and thus the dip of CT numbers is deepened and widen.

Now fracture aperture can be correlated with the integrated CT signal for those values identified under the minimum CT Number for matrix.

After calculating areas for different feeler gauges, plot of integrated CT signal versus aperture size shows a linear relationship as it can be seen in Figure 6.8.

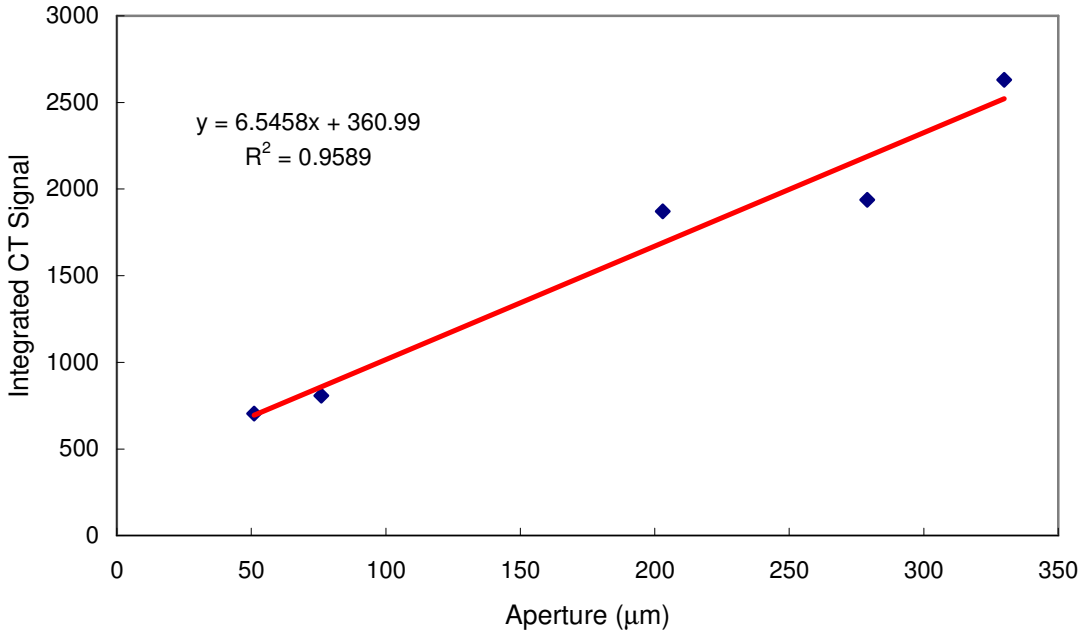

Figure 6.8 – Integrated CT signal vs. fracture aperture.

Once fracture aperture was measure a long the core, these values were found lognormal distributed. It is distributed with mean value of 22 μm and standard deviation of 500.

This fracture aperture data can be converted to fracture permeability by the following equation[32]

$$k_f = 8.45 \times 10^9 w^2 \quad [md]$$

where, w is in microns.

This distribution will be converted into fracture permeability via cubic law equation. The calculated fracture permeability then could be used as input data in dual porosity simulation model.

However there is no methodology to upscale fracture permeability values calculated in a core sample (micro scale) to reservoir simulations models (macro scale). Therefore, we

randomly generated several fracture permeability models using a lognormal distribution. Different minimum and maximum values between 1000 and 100000 mD were used to avoid unrealistic permeability values that may cause reservoir simulation calculations instability.

After several simulation runs using different fracture permeability distributions we found that the model with fracture permeability values between 20000 mD to 40000 mD shows a better match to observed data (Figure 6.9).

As a result, an additional improvement in the water production rates was obtained as show in CASE-6 model (Figure 6.10).

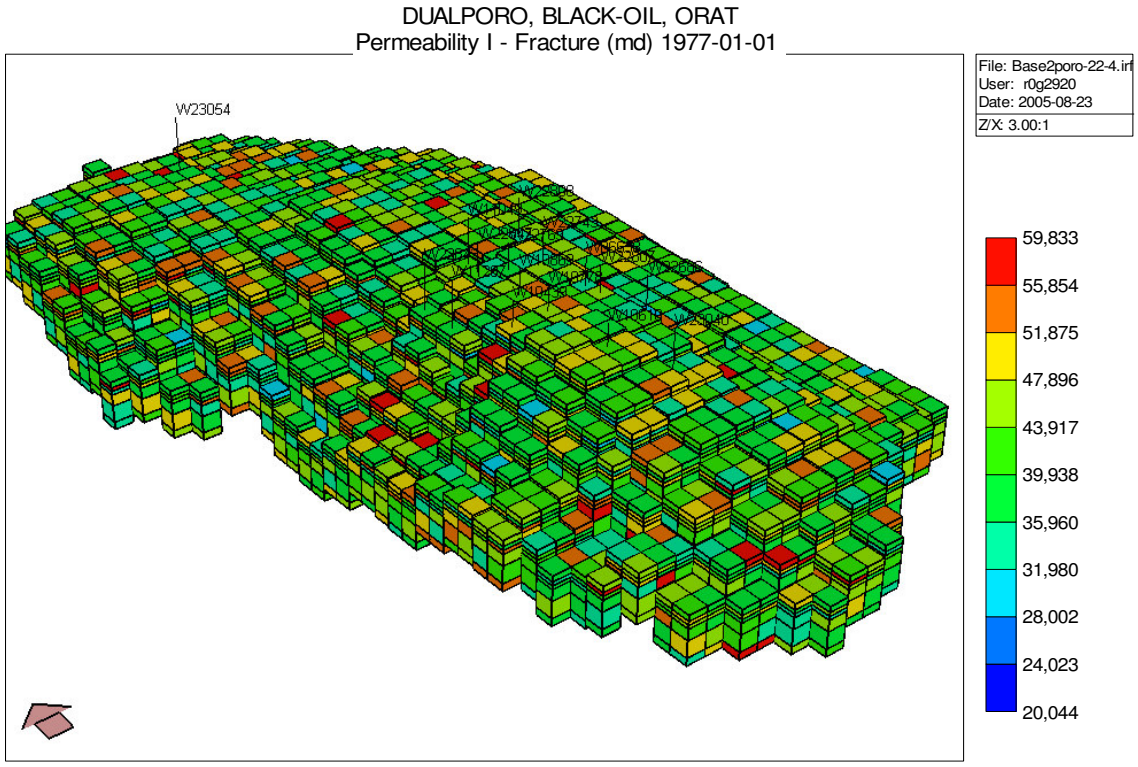

Figure 6.9 – Variable fracture permeability model.

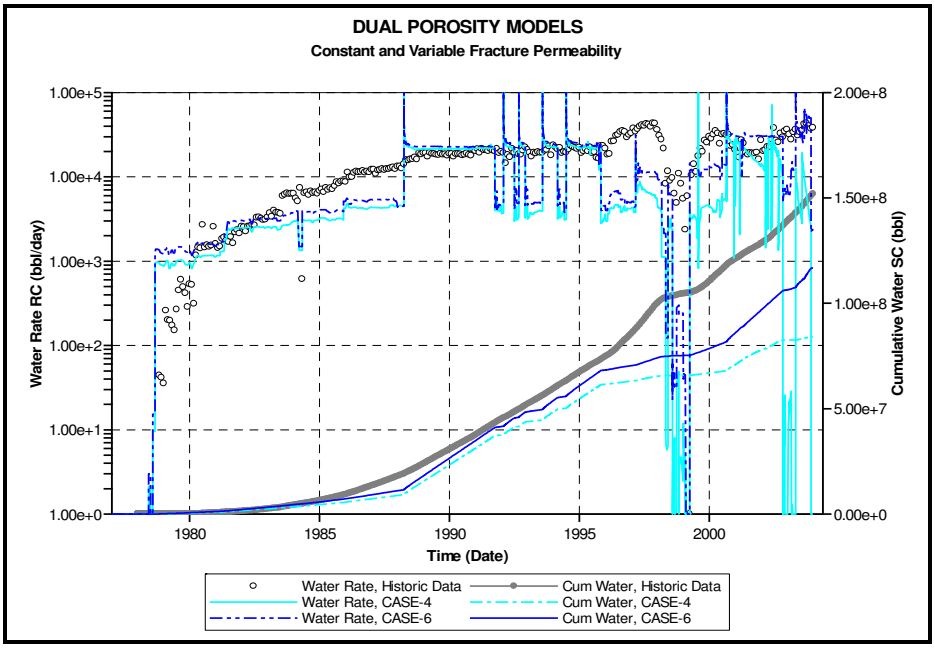

Figure 6.10 - Water production, dual porosity models with constant and variable Kf.

Once the simulation CASE-6 was obtained, additional modifications in fracture permeability around the wells were necessary to match field production rates (Figure 6.11). Although the cumulative water production of the field could not be exactly matched, we considered that the model represents the current reservoir water saturation conditions because the good match achieved in water production rates for the last 5 years.

All the wells were completed in the layer 4, the main producing interval in Tensleep Formation. In order to match fluids production, in some wells were necessary to complete either upper or lower layers.

Most of the wells are currently producing at a water cut of 99%, (Figure 6.12). Tensleep Formation is currently at residual oil saturation conditions, if the by-passed oil is not considered.

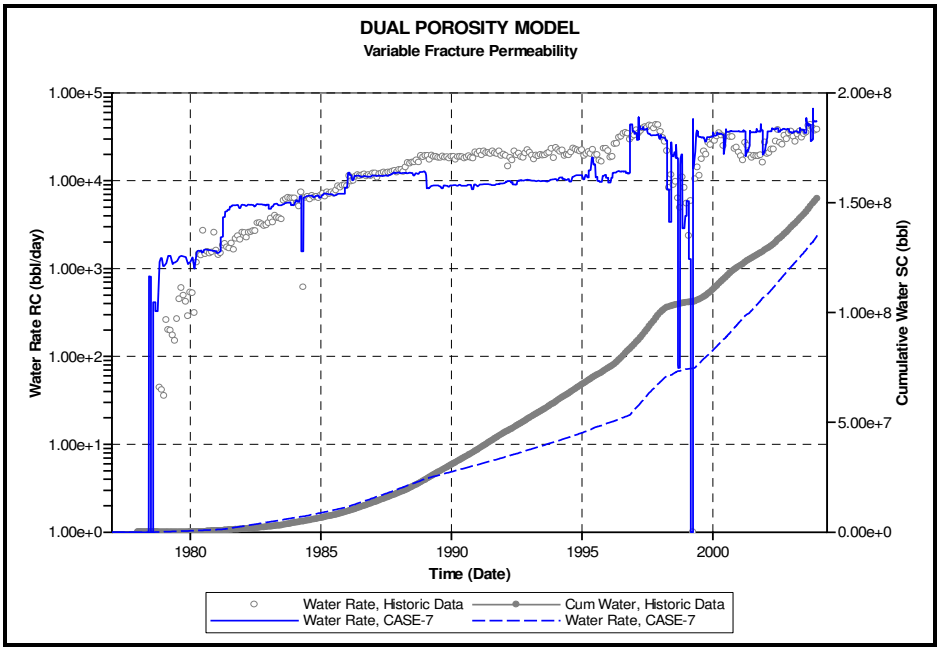

Figure 6.11 - Water production history match.

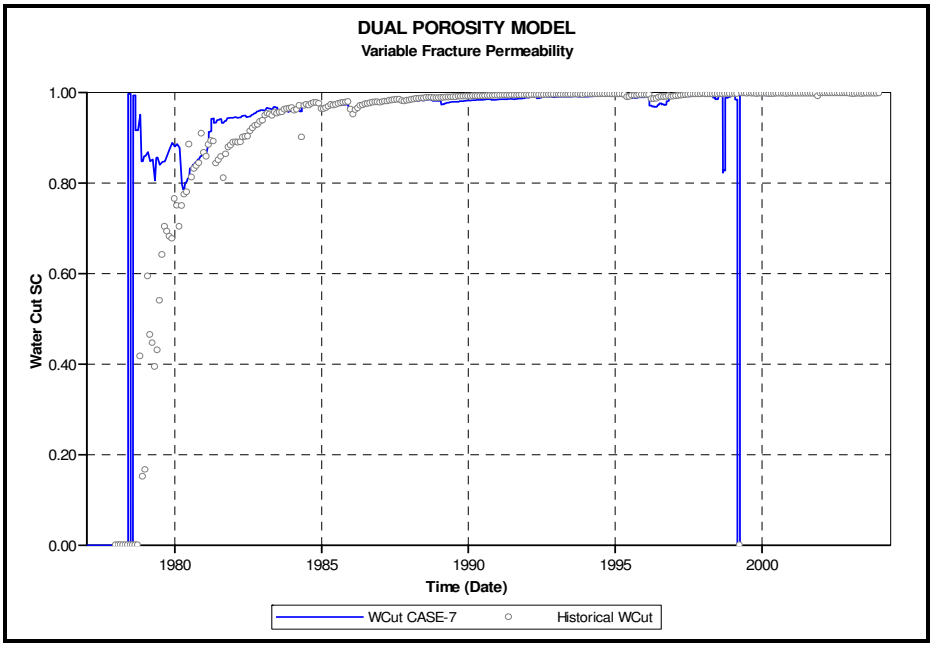

Figure 6.12 - Water cut history match.

In most of the wells, a good match of oil and water rates was obtained. Figures 6.13 to 6.15 show examples of history match in some wells.

Based on these results, we considered that the simulation model has been properly calibrated and furthermore it can be used to run prediction cases.

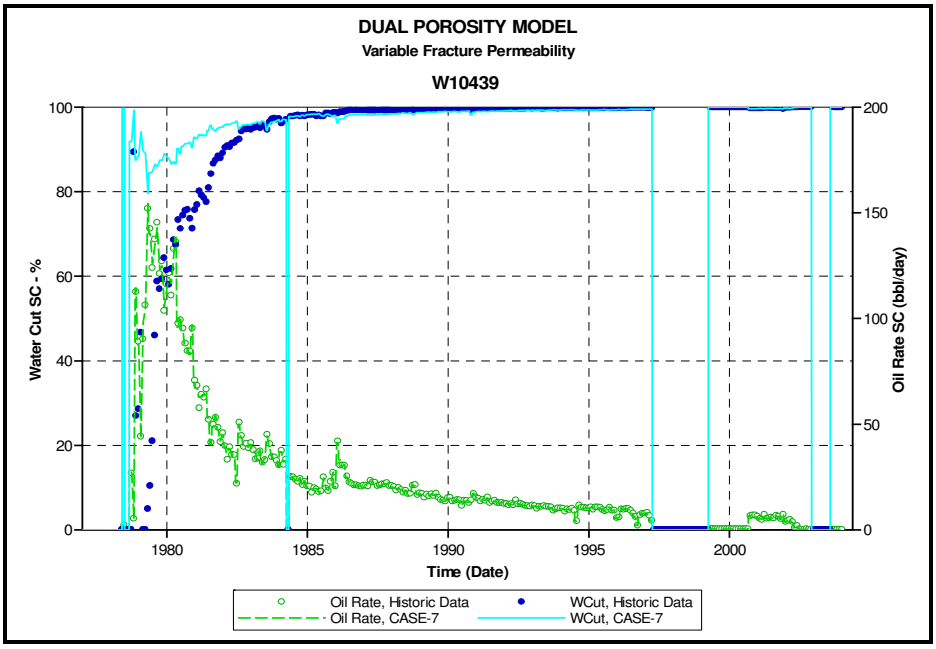

Figure 6.13 - History match in Well W10439.

Lack of information related with location of perforated intervals in previous Tensleep zones division and the simplified homogeneous geological model difficult to match the observed data.

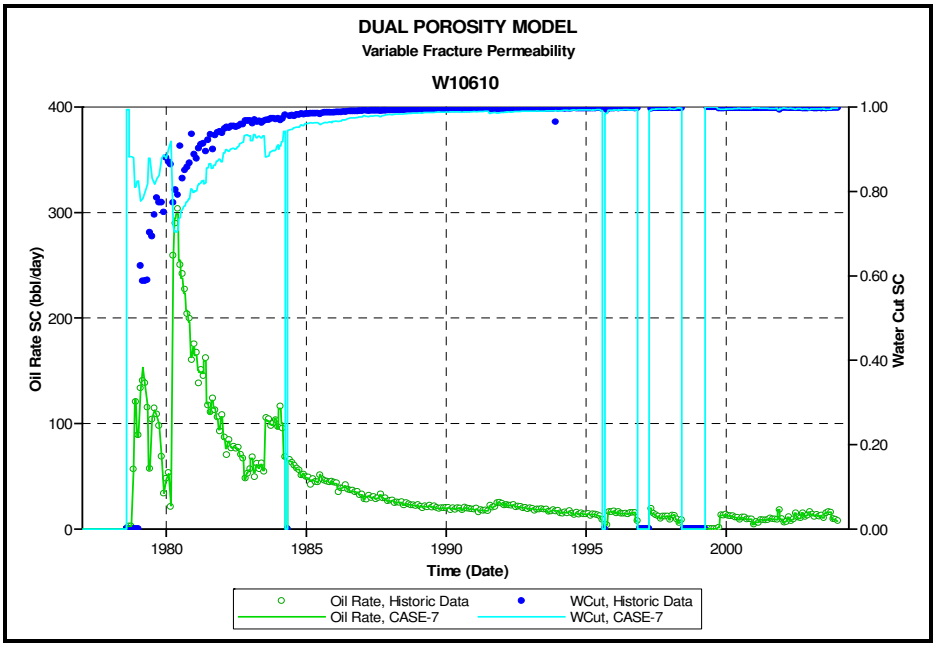

Figure 6.14 - History match in Well W10610.

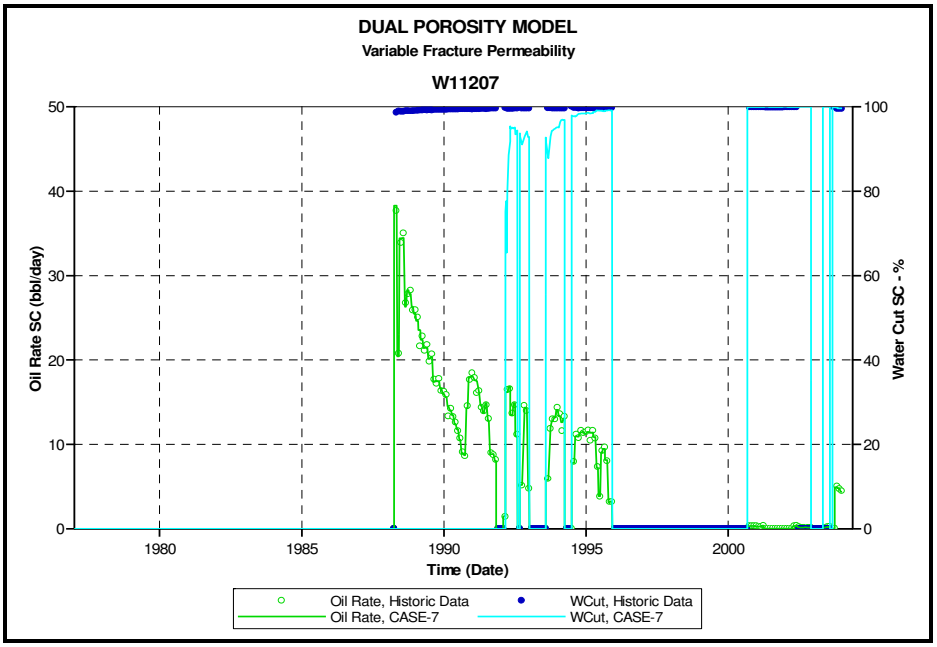

Figure 6.15 - History match in Well W11207.

In the simulation model, Tensleep Formation initially contained 5.8 MMSTBO. At the end of the history match period, 1.52 MMSTB have been produced or 26% of the OOIP. The remaining oil in place is 4.28 MMSTBO. Despite the high water cut in all the wells, the average remaining oil saturation at the end of the history match was 40%.

Water breakthrough in the wells through the fracture system, his causes a non-uniform advance of the water front and therefore poor sweep efficiency. High-permeability fractures ease water breakthrough earlier than the low-permeability fractures, leaving some untapped oil reserves behind.

6.3 History Matching Using Compositional and Pseudo-Miscible Simulation

A full field simulation model was generated to obtain current saturation conditions using the geological grid of CASE-7 and the compositional fluid model described in Chapter V. Unfortunately, in this field compositional simulation case (CASE-8), very small time steps are necessary and the numerical solution procedure asked for non practical computer memory to reach a solution. High material balance errors, around 20% in the gas were observed. Several attempts to correct the compositional model increasing available computer memory for the simulation were unsuccessfully tested.

A CASE-9 was run using the pseudo-compositional fluid model. As in the CASE-8, pseudo-miscible model showed calculation difficulties at field scale. Reservoir fluid model appear to be confident and reliable, however no improvement in the simulation time and stability was possible.

CHAPTER VII

ENHANCED OIL RECOVERY AND CO_2 STORAGE EVALUATION

In this chapter, the enhanced oil recovery and CO_2 storage process evaluation is discussed. Several problems were obtained running the dual porosity field simulation model either with compositional or pseudo-miscible fluid models.

Enhanced oil recovery evaluation was perform using the quarter pattern model described Chapter V. This model was converted to dual porosity model and CO_2 injection rate sensitivity was evaluated.

CO_2 storage process was calculated at the breakthrough time and scaled to field size.

7.1 Quarter Pattern Compositional Model

The quarter pattern model used in the comparison of compositional vs. pseudo-miscible simulators was convert to dual porosity and used in this evaluation, (Figure 7.1). Fracture permeability of 10000 mD was used. The model was initialized with matrix S_o = 40% and fracture S_o = 99% to represent the current saturation conditions in the reservoir. The possible by-passed oil is not considered in this evaluation; only additional recovery due to residual oil saturation reduction is contemplated.

Compositional fluid models were used to represent the miscible process of enhanced oil recovery in Tensleep formation.

Synthetic model has a hydrocarbon pore volume of 208 MSTB.

To investigate the effect of CO_2 injection rate on the enhanced oil recovery process, five sensitivities cases were run. Injection rates at reservoir conditions of 100, 200, 300, 400 and MSCFD of CO_2 were used.

Formation fracture pressure was assumed to be the initial reservoir pressure, then maximum injection pressure of 2300 psi at the well head was specified in the injectors. Producer is constrained by bottom-hole pressure of 2000 psi.

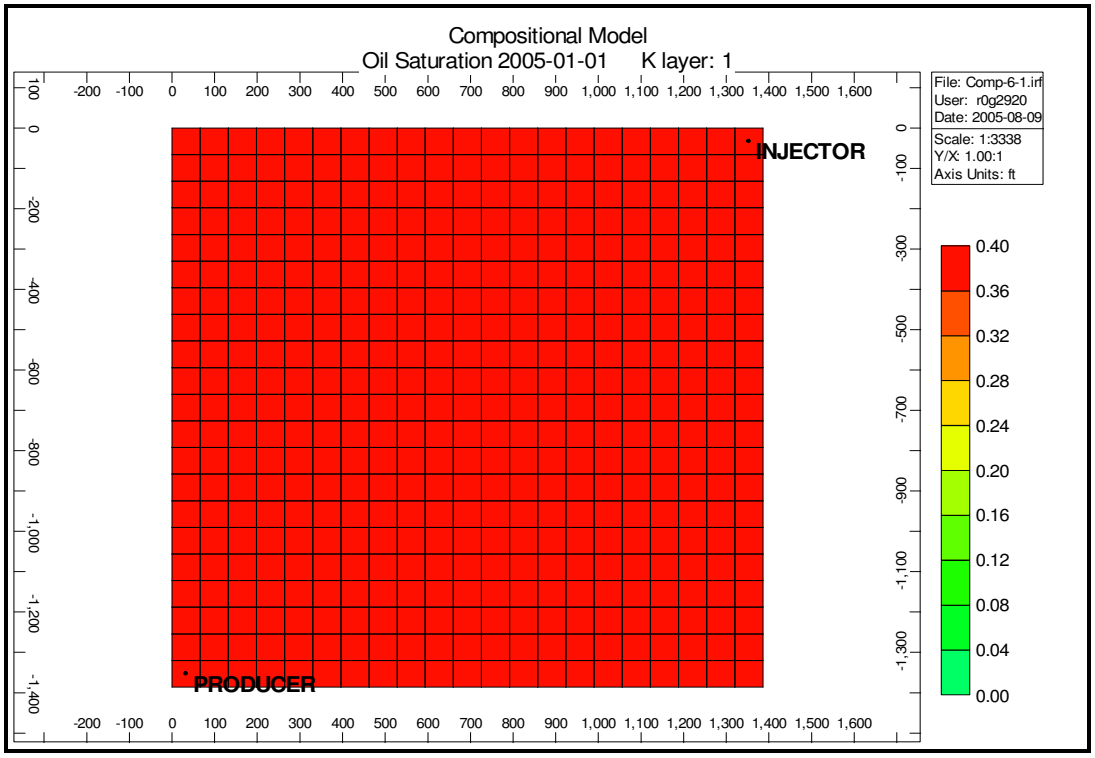

Figure 7.1 – Quarter pattern compositional model.

Injection gas rate sensitivity using compositional fluid model shows that at CO_2 volume injected of 0.6 PV, oil recovery decrease as injection rate increases, (Figure 7.2). Good oil recovery is observed in all injection cases.

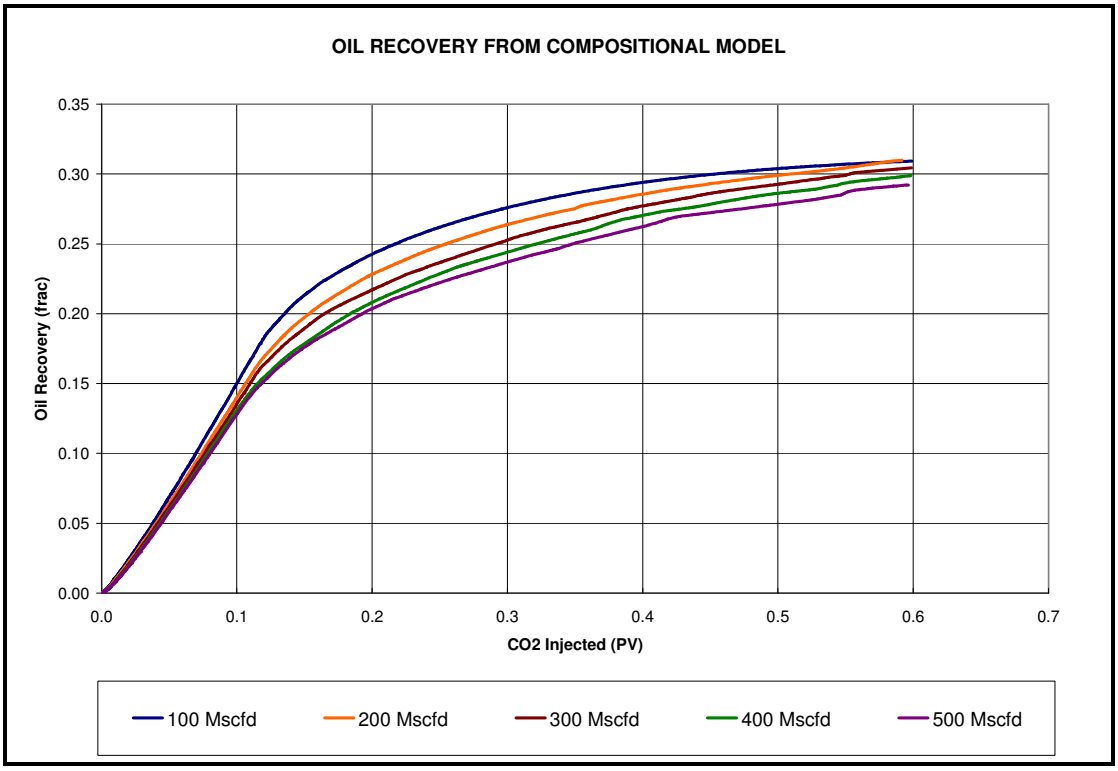

Figure 7.2 – Oil recovery from compositional model.

Comparison of final oil recovery as function of gas pore volume injected shows that a maximum recovery of 32% of the residual oil saturation can be obtained when gas is injected at 200 MSCFD, (Figure 7.3).

Acceleration in CO_2 gas breakthrough is observed when injection rate is increases. Dual porosity simulation models involve fractures; these fractures represent high permeability channels. These channels accelerate breakthrough of fluid with favorable mobility like CO_2.

These results can be used evaluate enhanced oil recovery at reservoir scale. Field simulation shows 33 times the quarter pattern hydrocarbon pore volume. Field model have an OOIP of 5.8 MMSTB. With a residual oil saturation of 40%, 2.32 MMSTB can be expected to remain in the reservoir.

Using the 32% of oil recovery, from the field scale approximately 0.7 MMSTB can be produced.

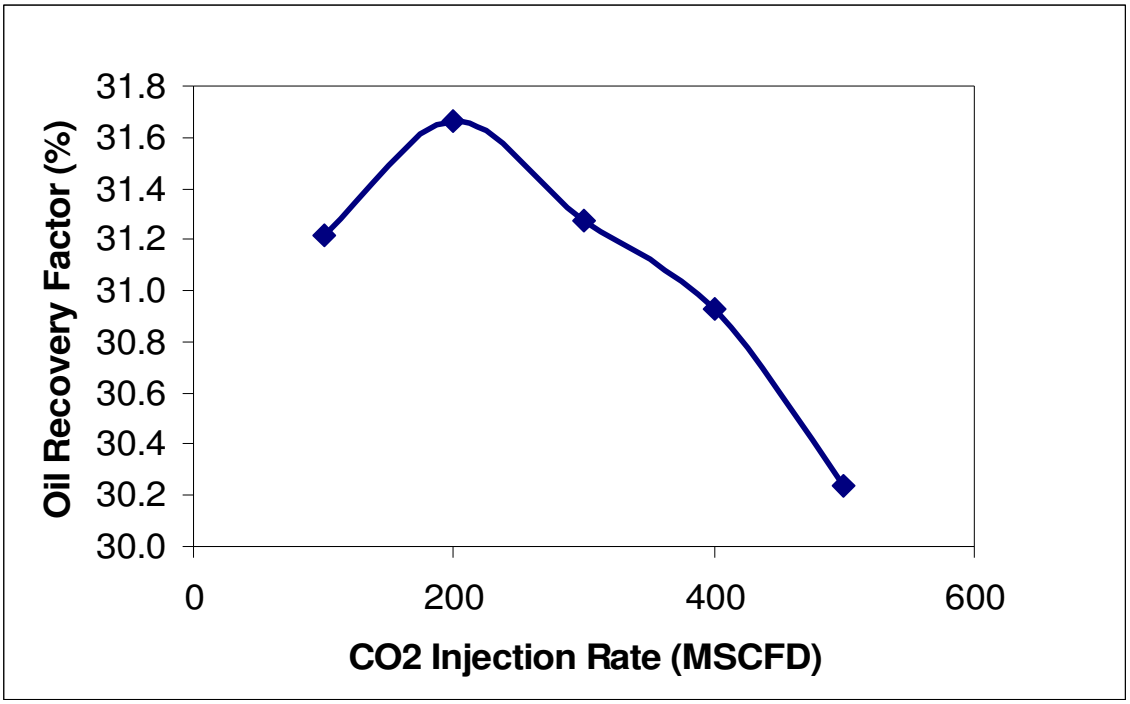

Figure 7.3 – Oil recovery as a function of injection rates.

CO_2 storage estimation for Tensleep Formation can be obtained in the same way form the quarter pattern model.

CO_2 breakthrough occurs at 18 months of continuous injection at 200 MSCFD, then at this time 109 MM SCF CO_2 were injected.

Theoretically extrapolating this value to reservoir scale we obtaining that 3597 MM SCFD of CO_2 can be storage in the reservoir.

7.2 Field Compositional Model

The dual porosity black oil simulation model used in the history match process was converted to compositional model. The no-lumped fluid model with 13 components was used in the evaluation.

The models start running without reporting any error in the simulation data file, this present calculation problems at the first day and the run can not continue.

Several attempts were made to run the compositional model changing different reservoir properties and conditions; however no stable runs could be obtained.

CHAPTER VIII

CONCLUSIONS

From the evaluation performed to the field data from Tensleep Formation, the next conclusions can be derived:

1. Compositional simulation should be used to evaluate CO_2 injection process.
2. Pseudo-miscible model is not able to represent the miscible process between CO_2 and reservoir fluid in Tensleep Formation.
3. Variable fracture permeability lognormal distributed depicts better the water advance thorough the highly fractured Tensleep Formation.
4. Additional PVT experiments like constant composition expansion and differential liberation are necessary to improve the hydrocarbon model.
5. A maximum of 32% of the residual oil volume can be recovered from a quarter pattern reservoir model when CO_2 is injected at 200 MSCFD.
6. 3597 MM SCFD of CO_2 can be storage in Tensleep Formation using the quarter pattern analogy.

8.1 Recommendations

7. Velocity information should be acquired in Teapot Dome in order to improve the geological model.
8. Sealing capacity of faults should be evaluated to improve the CO_2 storage capacity in Tensleep Formation.

9. For future field compositional simulation evaluation, lumped and no-lumped fluid samples should be tested.

10. Techniques to upscale fracture permeability values from cores to dual porosity simulation models should be evaluated.

11. Use of field simulation model in CO_2 storage evaluation in Tensleep Formation is necessary to know field response under different injection/production scenarios.

NOMENCLATURE

Z = gas deviation factor

ϕ = porosity

K = permeability, mD.

μ = viscosity, cp

ρ = fluid density, lb_m/ft^3

σ = interfacial tension

θ = contact angle.

FVF= formation volume factor

GOR=Gas-oil ratio

Subscripts

g = gas

w = water

o = oil

f = fracture

m = matrix

REFERENCES

1. Olsen, D.K., Sarathi, P.S., Hendricks, M.L., Schulte, R.K., Giangiacomo, L.A.: "Case History of Steam Injection Operations at Naval Petroleum Reserve No. 3, Teapot Dome Field, Wyoming: A Shallow Heterogeneous Light-Oil Reservoir," paper SPE 25786 presented at the 1993 International Thermal Operations Symposium, Bakersfield, CA, 8-10 February.

2. Curry, W.: "Teapot Dome – Past, Present and Future," *AAPG Bulletin* V. **61** No. 5 (May 1977), 671.

3. Martin, F.D. and Taber, J.J.: "Carbon Dioxide Flooding," *SPE Technology Today Serie*s (April 1992) 396 – 400.

4. Jarrel, P.M., Fox, C.E., Stein, M.H. and Webb, S.L.: F.: *Practical Aspects of CO_2 Flooding,* Monograph Series, SPE, Richardson, TX (2002).

5. Grigg, R.B.: "Long Term CO_2 Storage Using Petroleum Industry Experience," final technical report, CCP Subcontract # 3961, U.S. DOE, Washington DC (December 2002).

6. Options for CO_2 Storage, IEA Greenhouse Gas R&D Programme, www.ieagreen.org.uk/4.pdf, July 2005.

7. "Carbon Sequestration R&D," U.S. DOE, www.fossil.energy.gov/programs/sequestration/, June 2005.

8. Sanchez, N.L.: "Management of Water Alternating (WAG) Injection Projects," paper SPE 53714 presented at the 1999 Latin American and Caribbean Petroleum Engineering Conference, Caracas, Venezuela, 21-23 April.

9. Kulkarni, M. M. and Rao, D. N.: "Experimental Investigation of Various Methods of Tertiary Gas Injection," SPE 90589, paper presented at the 2004 Society of Petroleum Engineers Annual Technical Conference and Exhibition, Houston, TX, September 26 -29.

10. Rogers, J.D., Reid B. and Grigg, R.B.: "A Literature Analysis of the WAG Injectivity Abnormalities in the CO_2 Process," paper SPE 59329 presented at the 2000 Improved Oil Recovery Symposium, Tulsa, OK, 3-5 April.

11. Bennion, D.B., Thomas, F.B., Jamaluddin, A.K.M. and Ma, T.: "The Effect of Trapped Critical Fluid Saturations on Reservoir Permeability and Conformance," paper presented at the 1998 Annual Technical Meeting of the Petroleum Society of CIM, Calgary, Alberta, Canada, 8 -10 June.

12. Cooper, S.P., Lorenz, J.C. and Goodwin, L.B.: 'Lithologic and Structural Controls on Natural Fracture Characteristics Teapot Dome, Wyoming," Sandia Report, contract No. DE-AC04-94AL85000, U.S. DOE , Albuquerque, NM (June 2001).

13. Ennis-King, J. and Paterson, L.: "Engineering Aspects of Geological Sequestration of Carbon Dioxide," paper SPE 77809 presented at the 2002 Asia Pacific Oil and Gas Conference and Exhibition, Melbourne, Australia, 8-10 October.

14. Krumhansl, J., Pawar R., Grigg R., Westrich H., Warpinski N., *et al*.: "Geological Sequestration of Carbon Dioxide in a Depleted Oil Reservoir," paper SPE 75256 presented at 2002 SPE/DOE Improved Oil Recovery Symposium, Tulsa, OK, 13-17 April.

15. Schulte, R.: "Airborne Survey," final report, contract No. DOE/RMOTC – 020139, Casper, WY (June 2001).

16. Teapot Dome Geological Column, Rocky Mountain Oil Field Testing, www.rmotc.com/Facilities/Geo-sample.html, July 2005.

17. Zhang, Q., Nummedal, D. and Yin, P.: "Stratigraphy, Sedimentology and Petrophysics of the Tensleep Sandstone at Teapot Dome and in Outcrop," http://aapg.confex.com/aapg/rm2005/techprogram/A100171.htm, June 13 2005.

18. Zhang, Q., Nummedal, D. and Yin, P.: "Reservoir Heterogeneity Caused by Diagenesis in Tensleep Sandstones, Teapot Dome, Wyoming," presented at the 2005 AAPG Annual Meeting, Calgary, Alberta, Canada, June 19-22.

19. IMEX, Version 2004.11, User Manual, Computer Modeling Group, Calgary (2004).

20. GEM, Version 2004.10, User Manual, Computer Modeling Group, Calgary (2004).

21. Todd, M.R. and Longstaff, W.J.: "The Development, Testing, and Application of a Numerical Simulator for Predicting Miscible Flood Performance," paper SPE 3484, *JPT* (July 1972) 874.

22. Muralidharan, V., Chakravarthy, D., Putra, E., and Schechter, D.S.: "Investigating Fracture Aperture Distributions under Various Stress Conditions Using X-Ray Scanner," paper CIPC 2004-230 presented at 2004 Annual Technical Meeting of the Petroleum Society, Calgary, Alberta, Canada, 8-10 June.

23. McDonald A.E., Beckner, B.L., Chan, H.M., Jones, T.A., Wooten, S.O.: "Some Important Considerations in the Simulation of Naturally Fractured Reservoirs," SPE 21814, presented in Rocky Mountain Regional Meeting and Low-Permeability Reservoirs Symposium, Denver, CO, April 15-17, 1991.

24. Merrill, R.C., Hartman, K.J. and Creek, J.L.: "A Comparison of Equation of State Tuning Methods," paper SPE 28589 presented at the 69th Annual Technical and Exhibition New Orleans, LA, 25-28 September.

25. Khan, S.A., Pope, G.A. and Sepehrnoori, K.: "Fluid Characterization of Three-Phase CO_2/Oil Mixtures," paper SPE/DOE 24130 presented at the 8th Symposium Oil Recovery, Tulsa, OK, 22-24 April, 1992.

26. Peng, D.Y. and Robinson, D.B.: "A New Two-Constant Equation of State," *Ind. & Eng. Chem. Fund.* (1976) **15**, No. 1, 59-64.

27. Lohrenz, J., Bray, B.G. and Clark, C.R.: "Calculating Viscosities of Reservoir Fluids from Their Compositions," *JPT* (Oct. 1964) **16**, 1171-1176.

28. Whitson, C.H.: "Characterizing Hydrocarbon Plus Fraction," *SPEJ,* **23**, 1983, 683-684.

29. Aguilar, R.A. and McCain, W.D.: "An Efficient Tuning Strategy to Calibrate Cubic EOS for Compositional Simulation," paper SPE 77382 presented at the 2002 Annual Technical Conference and Exhibition, San Antonio, TX, 29 September – 2 October

30. Simon, R. and Graue, D.J.: "Generalized Correlations for Predicting Solubility, Swelling and Viscosity Behavior of CO_2 -Crude Oil Systems," paper SPE 917, *JPT* (January 1965) 102.

31. Fevang, O., Singh, K. and Whitson, C.H.: "Guidelines for Choosing Compositional and Black-Oil Models for Volatile Oil and Gas Condensate Reservoirs," paper SPE 63087 presented at the 2000 SPE Annual Technical Conference and Exhibition, Dallas, TX, 1-4 October.

32. Witherspoon, P.A., Wang, J.S.Y., Iwai, K. and Gale, J.E.: "Validity of Cubic Law for Fluid Flow in a Deformable Rock Fracture," *Water Resources Research,"* (1980) V. **16** No. 6, 1016-1024.

VITA

Name:	Ricardo Gaviria Garcia
Permanent Address:	Harold Vance Department of Petroleum Engineering. Texas A&M University 507 Richardson Building College Station, TX 77843-3116, U.S.A.
Email:	ricardo.gaviria@tamu.edu
Education:	B. S., Petroleum Engineering, Universidad Industrial de Santander, Bucaramanga, Colombia (November 1998) M.S., Petroleum Engineering Texas A&M University College Station, TX 77843-3116, U.S.A. (December 2005)